Air-To-Ground NOMA Systems for the "Internet-Above-the-Clouds"

Panagiotis Botsinis, *Member, IEEE,* Dimitrios Alanis, *Member, IEEE,* Chao Xu, *Member, IEEE,* Zunaira Babar, Daryus Chandra, Soon Xin Ng, *Senior Member, IEEE,* and Lajos Hanzo, *Fellow Member, IEEE*

***Abstract*—The provision of high-speed Internet access in aircraft is mainly supported by satellite links at the time of writing, aided by links between the aircraft and the ground stations. It is anticipated that Air-To-Ground (A2G) communications between en-route aircraft and the ground stations will have a major role in providing the required Quality of Service, while complying with the low latency requirements of next generation of communications networks. Non-Orthogonal Multiple Access (NOMA) systems will increase the system throughput by allowing multiple aircraft to simultaneously communicate with the ground station, while requiring fewer resource slots. Given the limited number of orthogonal resource 'slots' and the high number of aircraft to be supported, a potentially high level of interference is expected. In this contribution, we employ beamforming based on the Angle of Arrival (AoA) of the signals and antenna arrays having multiple antenna elements, as well as a novel interference-exploiting Sphere Decoder (iSD), which detects the signals of the supported users, while beneficially exploiting those of the interfering users. We show that an improved performance may be achieved in both Hard-Input Hard-Output (HIHO) scenarios, as well as in iterative Soft-Input Soft-Output (SISO) scenarios, when compared to the conventional Sphere Decoder, the Maximum Likelihood (ML) detector and the Maximum *A posteriori* Probability (MAP) detector. We also characterize the complexity of the proposed receiver and evaluate its performance with the aid of BER simulations and EXtrinsic Information Transfer (EXIT) charts.**

***Index Terms*—aircraft communications, algorithm design and analysis, beamforming, multiuser detection, non-orthogonal multiple access, optimization, sphere decoder, wireless communication**

I. Introduction

Passenger aircraft remain one of the few places, where high-speed and low-latency connectivity is not a widely available commodity at the time of writing [1], despite the demand for high-throughput low-latency communications [2]. At the current state-of-the-art, Internet access on aircraft is mainly supported by satellite links, while, additionally, being aided by Air-To-Ground (A2G) communications between the aircraft and a Ground Station (GS). However, the links between satellites and airplanes suffer from a high end-to-end latency [3]. Aeronautical Ad-hoc NETworks (AANET) may be capable of mitigating the latency of communications to aircraft [4]–[6]. In AANETs, the aircraft may convey information to each other in an ad-hoc fashion and based on optimized routing algorithms.

The A2G link of AANETs may have the role of the sink or gateway in order for the aircraft to connect to the Internet [1]. At the same time, the A2G link has a lower delay than satellite communications, making it a better candidate for delay-sensitive applications, such as live video and audio streaming, as well as for emergency and control signals. Another advantage of A2G communications is that an A2G provider is associated with a significantly lower cost than a satellite provider [7].

AANETs may be viewed as relatives of terrestrial VANETs, hence they have a number of similarities, such as more predictable motion trajectories than pedestrians and the increased need for improved security, privacy, scheduling and routing. However, AANETs and VANETs also differ in various aspects, such as for example the Doppler speed of the served users and interferers, their potentially low-quality sporadic connectivity, as well as their more dynamic network topology. The applicability of VANET protocols in AANETs has been investigated in [8].

There is a number of A2G systems deployed, each focusing on different applications, operating at different frequencies and offering diverse throughput values [1]. Table I gathers the current A2G systems, which focus on data transmission, along with a short description.

Therefore, multiple aircraft have to be supported simultaneously by a GS in order to provide the expected Quality of Service (QoS). At the time of writing, Orthogonal Multiple Access (OMA) is being used in all releases of mobile communications, where all supported users are separated using orthogonal resources, such as different time slots, carrier frequencies or orthogonal codes. Non-Orthogonal Multiple Access (NOMA) [19]–[23] is expected to increase a system's achievable throughput compared to an OMA system, because it allows more users to be supported by the network than the limited number of orthogonal resources available. The cost of higher throughput in NOMA systems is higher detection complexity imposed on the GS than that of OMA systems. More precisely, in a synchronous A2G NOMA system, there are multiple signals arriving simultaneously at the GS transmitted by the supported users. Therefore, the GS has to jointly detect and decode the signal transmitted by each of the supported users. By using the full-search based Maximum Likelihood (ML) Multi-User Detector (MUD) or the Maximum *A posteriori* Probability (MAP) MUD, the detection

The authors are with the School of Electronics and Computer Science, University of Southampton, Southampton, SO17 1BJ, UK (email: {pb1y14, da4g11, cx1g08, zb2g10, dc2n14, sxn, lh}@ecs.soton.ac.uk).

The financial support of the European Research Council under the Advanced Fellow Award QuantCom, that of the Royal Society's Wolfson Research Merit Award and that of the Engineering and Physical Sciences Research Council under Grant EP/Noo4558/1, EP/PO34284/1 is gratefully acknowledged. The use of the IRIDIS High Performance Computing Facility at the University of Southampton is also acknowledged.

TABLE I: Air-To-Ground (A2G) Systems

System	Description
Aircraft Communication Addressing and Reporting System (ACARS) [9]	In use since 1978. Secure and authenticated exchange of short messages between the aircraft and the GS via HF, VHF or satellite links. It is not suitable for high-throughput, low-latency communications.
SELective CALling (SELCAL) [10]	Introduced in 1957. Suitable for voice transmissions over HF and VHF. Not suitable for delay-critical communications.
L-band Digital Aeronautical Communication System 1 (L-DACS1) [11], [12]	A Frequency Division Duplexing (FDD) multi-carrier system using Orthogonal Frequency Division Multiplexing (OFDM). It is an amalgamation of the Broadband Aeronautical Multi-Carrier Communications (B-AMC) [13] and of the WorldWide interoperability for Microwave Access (WiMAX) [14]. It is scalable, spectral-efficient, flexible, and suitable for voice communications.
L-band Digital Aeronautical Communication System 2 (L-DACS2) [15], [16]	A Time Division Duplexing (TDD) system, which is suitable for asymmetric data traffic. It is a combination of the Global System for Mobile communications (GSM), of the All-purpose Access Transceiver (UAT) and of the All-purpose Multi-channel Aviation Communication System (AMACS).
European Aviation Network (EAN) [17]	S-band satellite and Long-Term Evolution (LTE) GSs operated by Inmarsat and Deutsche Telekom for supporting the european aeronautical networks. There are 300 GSs in the European Union, which are able to provide a network capacity of up to 50 Gbps.
Gogo A2G Network [18]	Network consisting of 200 GSs in USA and Canada, providing high-speed internet to commercial aircraft up to 9.8 Mbps.

complexity increases exponentially with the number of aircraft supported. Therefore, low-complexity detectors, such as the Sphere Decoder (SD) [24]–[30] may be used for achieving near-optimal performance, while requiring only a fraction of the optimal detectors' complexity.

The NOMA principle may be applied in diverse system configurations, for example in the context of beam-forming, spatial division multiple access (SDMA), code division multiple access (CDMA), interleave division multiple access (IDMA), etc. Hence it may be readily used for all communications systems to improve delay-critical low-latency applications by serving the users more promptly. Therefore the NOMA principle may also be viewed as an 'add-on' technique of improving the throughput of the OMA philosophy, for example by assigning two or more users to the same time-, frequency- or spatial-domain 'resource-slot' at a different power-level, which can then be separated by the receiver at the cost of some extra receiver-complexity.In the context of A2G and AANET communications, NOMA may be employed for the same reasons as in terrestrial VANET or pedestrian systems, but additionally taking into consideration the fact that the mobile speed is higher, the topology fluctuates more dynamically, the propagation distances are higher and the communication channels are different.

A2G systems may also be benefited by the use of Multi-Functional Antenna Arrays (MFAA) [31]. More specifically, an Antenna Array (AA) at the GS may use its Antenna Elements (AE) for performing adaptive receive beamforming [32], essentially nulling the interferers' signals, given that the Angle of Arrival (AoA) of each signal has been accurately estimated. In high-frequency NOMA systems, digital adaptive beamforming is expected to be essential, since it increases the throughput of the users supported.

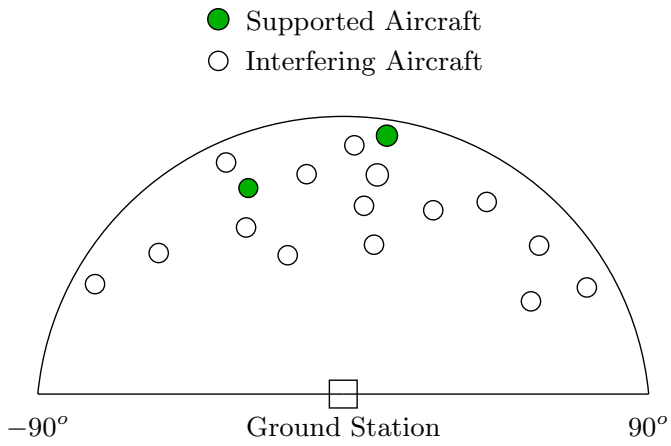

Fig. 1: The A2G scenario considered in this paper. Multiple supported aircraft have to convey their information to the GS in the midst of interference. The GS's service is extended from -90^o to 90^o, while the angular position as well as the distance of the aircraft is assumed to be perfectly estimated.

Against this background, our novel contributions are:

1) *We investigate a rank-deficient A2G NOMA system, where there are more supported and interfering users than the number of AEs on each receive AA. Adaptive beamforming is employed for cancelling out the inter-*

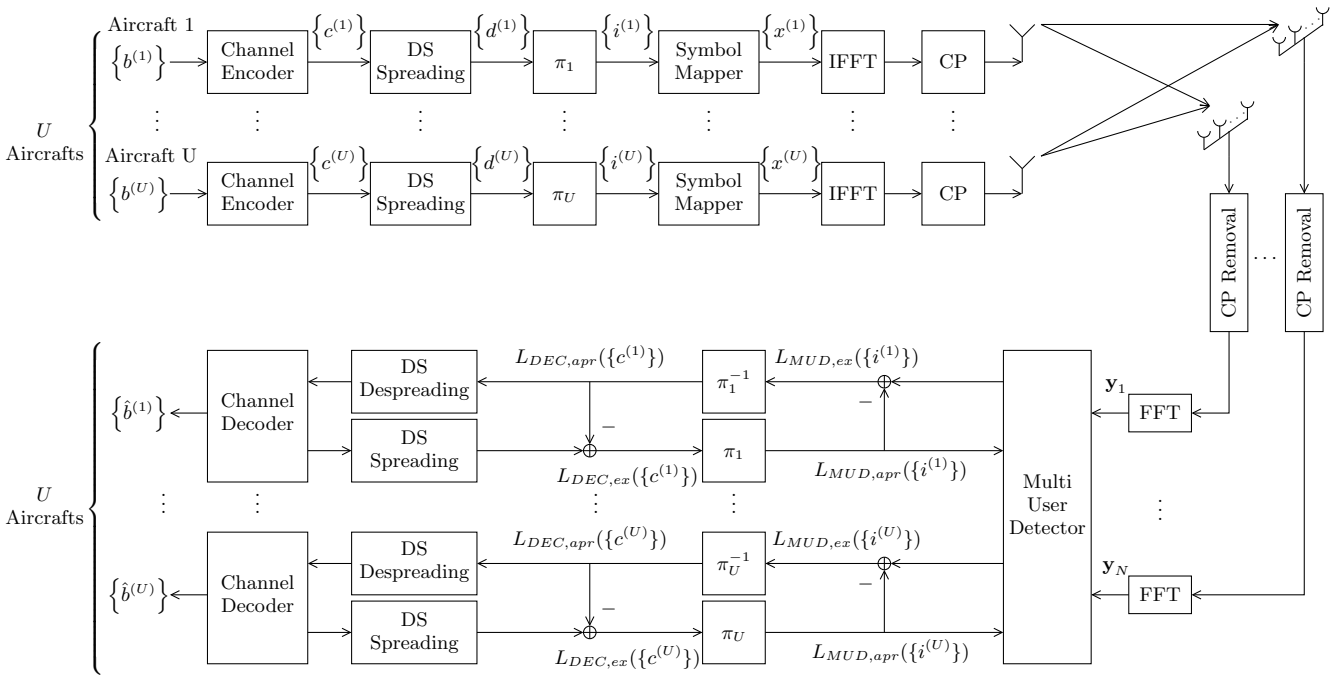

Fig. 2: The MC-IDMA A2G communication system's block diagram of the aircraft and the GS employing recursive systematic convolutional coding and direct sequence spreading, in association with iterative detection and decoding at the GS.

ferers based on their angular position.

2) *We propose novel Hard-Input Hard-Output (HIHO), as well as iterative Soft-Input Soft-Output (SISO) interference-exploiting SDs (iSD), inspired by the Radial Basis Function (RBF)-aided equalization [33], [34], which take into consideration the signals transmitted by the interferers. Due to the system being rank-deficient, there may be interfering signals that are not sufficiently attenuated by the adaptive receive beamformer. These interfering signals may assist us in achieving an improved detection of the supported users' signals.*
3) *We compare the proposed iSDs to the optimal ML and MAP detectors, as well as to the conventional HIHO and SISO SDs. We evaluate their performance with the aid of 3D Bit Error Ratio (BER) and complexity surfaces. When iterations are allowed between the MUD and the channel decoder, as in the case of the SISO iSD, the SISO SD and the MAP MUD, the system's performance is evaluated with the aid of EXtrinsic Information Chart (EXIT) charts. We demonstrate that an improved performance may be achieved with the aid of HIHO and SISO iSDs, albeit at a higher complexity than that of the corresponding SDs.*

The paper is structured as follows. In Section II, the A2G NOMA system investigated is presented and characterised, including the adaptive beamforming method, as well as the MUD and iterative decoding process at the GS. In Section III we conceive the novel HIHO and SISO iSDs, which are then evaluated in Section IV in rank-deficient A2G NOMA systems. Finally, our conclusions are offered in Section V.

II. A2G System Model

The A2G scenarios that we consider in this contribution are depicted in Fig. 1. A GS is equipped with MFAAs for providing both beamforming and diversity gains. The angular position of the aircraft is assumed to be perfectly estimated and predicted, where U aircraft are supported by the GS. Additionally, there are U_{intrf} interfering aircraft, whose positions and communications systems are known as well, but they are not served by that specific GS. This may occur, when there are multiple GSs operated by the same provider, which are aware of the resource allocation and Adaptive Coding and Modulation (ACM) index that has been assigned to each link, but are programmed to serve only a subset of these aircraft. Therefore, for each GS, a different subset of the aircraft, relying on the same resources will be considered as the supported aircraft, with the rest of the aircraft being treated as interference. In our system model, the angular positions of the supported and interfering aircraft play an important role for determining whether NOMA or OMA will be employed. If the former is selected, the streams of the interfering aircraft that will participate in the demodulation are determined based on their angular vicinity to that of the supported aircraft. We believe that predicting the angular position at the ground station is a reasonable assumption, given that the routes of the aircraft are co-scheduled and known to the ground station. Please note that no high-accuracy estimate of the angular position is required for demodulation, since it only determines, which specific aircraft's streams will be jointly detected and demodulated.

The goal of the GS seen in Fig. 1 is to jointly decode the information bits of the U supported planes in the face of the noise and interference imposed by the U_{intrf} users,

with the aid of receive beamforming and MUDs. Throughout this manuscript, we have modelled the angular locations of the planes to be uniformly random, in order to evaluate the most general scenarios. In practice, the positions and routes of the aircrafts are expected to be carefully scheduled and known to the ground station. For instance, in the radar literature, it is very common to assume that the direction of arrival of a source is known, since the radars often perform their search using a relatively narrow beam. The beam is steered either mechanically or electronically in the azimuth and/or elevation domain to pinpoint targets [35]. If a return signal is detected by the receiver, then the current angle represents the direction of some object (an aircraft in our case). Furthermore, in the target tracking literature it is assumed that the radar acquires both range and azimuth (angle) measurements for a target to be tracked and it uses them as input information to track the object for example with the aid of a Kalman filter [36], [37]. This would improve the prediction capabilities of the ground station, allowing it to switch betweens NOMA and OMA more accurately.

A. Transmitters' System Model

Due to the plethora of existing aircraft that are eligible to be served by a GS, we have opted to use the Multi-Carrier Interleave Division Multiple Access (MC-IDMA) NOMA scheme [38]–[44]. The A2G system's block diagram is illustrated in Fig. 2. The uth supported aircraft initially encodes its information bit stream $\{b^{(u)}\}$ with the aid of a recursive systematic convolutional encoder having a coding rate R. The encoded bit stream $\{c^{(u)}\}$ is then spread by using a Direct-Sequence (DS) with a pre-determined Spreading Factor (SF). Afterwards, the encoded and spread bits $\{d^{(u)}\}$ are interleaved using a user-specific interleaving sequence.

The combination of bit-level spreading and the user-unique interleaving sequence makes IDMA attractive as a NOMA scheme. Please note, however, that other NOMA schemes, such as Sparse Code Multiple Access (SCMA), Pattern Division Multiple Access (PDMA) and Multi-User Shared Access (MUSA) may also be used in A2G NOMA systems, allowing them to transmit their streams over the same shared time-, frequency- and spatial resources [45]. In SCMA, each transmitted stream of each aircraft is mapped to a multi-dimensional sparse codeword, which is part of a specific codebook. This way, multiple supported users are able to use the same time- and frequency-domain resources in OFDMA. The ground station uses a Message Passing Algorithm (MPA) in order to recover the transmitted streams. The sparsity of the codewords exploits the near-optimal nature of the MPA. In Pattern Division Multiple Access, the users' data is scheduled in unique, user-specific patterns of time-, frequency- and spatial-domain resources in order to separate the users transmitting partially in the same time-, frequency- and spatial-domain resources. The sparsity of the user-specific patterns allows a low-complexity detector to be employed for detecting the users' signals. In Multi-User Shared Access, different portions of the available power budget is allocated to each supported user's signal, in order to exploit the users' topology

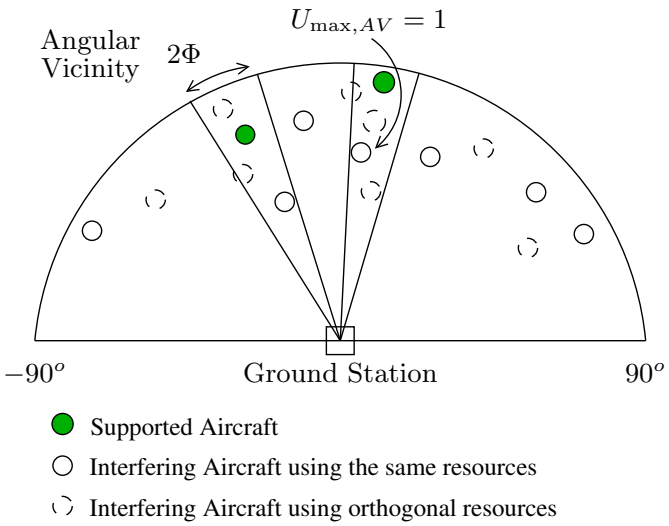

Fig. 4: The A2G scenario considered in this paper, when the aircraft have been separated orthogonally in the frequency or time domain, based on the configurable angular vicinity Φ of the supported aircraft and the maximum number of interfering aircraft that are allowed to use the same resources in that angular vicinity $U_{\max,AV}$.

and their channel quality. For example, a higher power would be allocated to a user who is at the edge of the coverage region, than that assigned to a user closer to the GS. Thse users may be readily separated by a Successive Interference Cancellation (SIC) aided receiver.

After the interleaved bit sequence $\{i^{(u)}\}$ is mapped to the symbols of a pre-determined modulation scheme, the symbol stream $\{x^{(u)}\}$ is mapped to subcarriers. The Inverse Fast Fourier Transform (IFFT) converts the symbol stream from the frequency domain to the time domain. A sufficiently long cyclic prefix is attached to the beginning of the OFDM symbol in order to protect the system from Inter-Symbol Interference (ISI).

B. Channel Model

The A2G channel may be modeled as a two-path channel [46]–[48], where the main path corresponds to the Line-Of-Sight (LOS) path and the second path models the reflections from the terrestrial environment. In [46] it was mentioned that all reflections arrive during the same delay bin in the Power Delay Profile (PDP) of the channel, hence they can be considered as a single Rayleigh fading process. Therefore, the power received from the LOS path may be calculated based on a free-space Path Loss (PL) model and it depends on the distance between each aircraft and the GS. The second path's average power is reduced even further than that of the LOS path, according to a Rician factor that characterizes a typical aeronautical scenario. In our contribution we will consider a power ratio between the LOS path and the reflected path of $K_{rice} = 15$ dB [46].

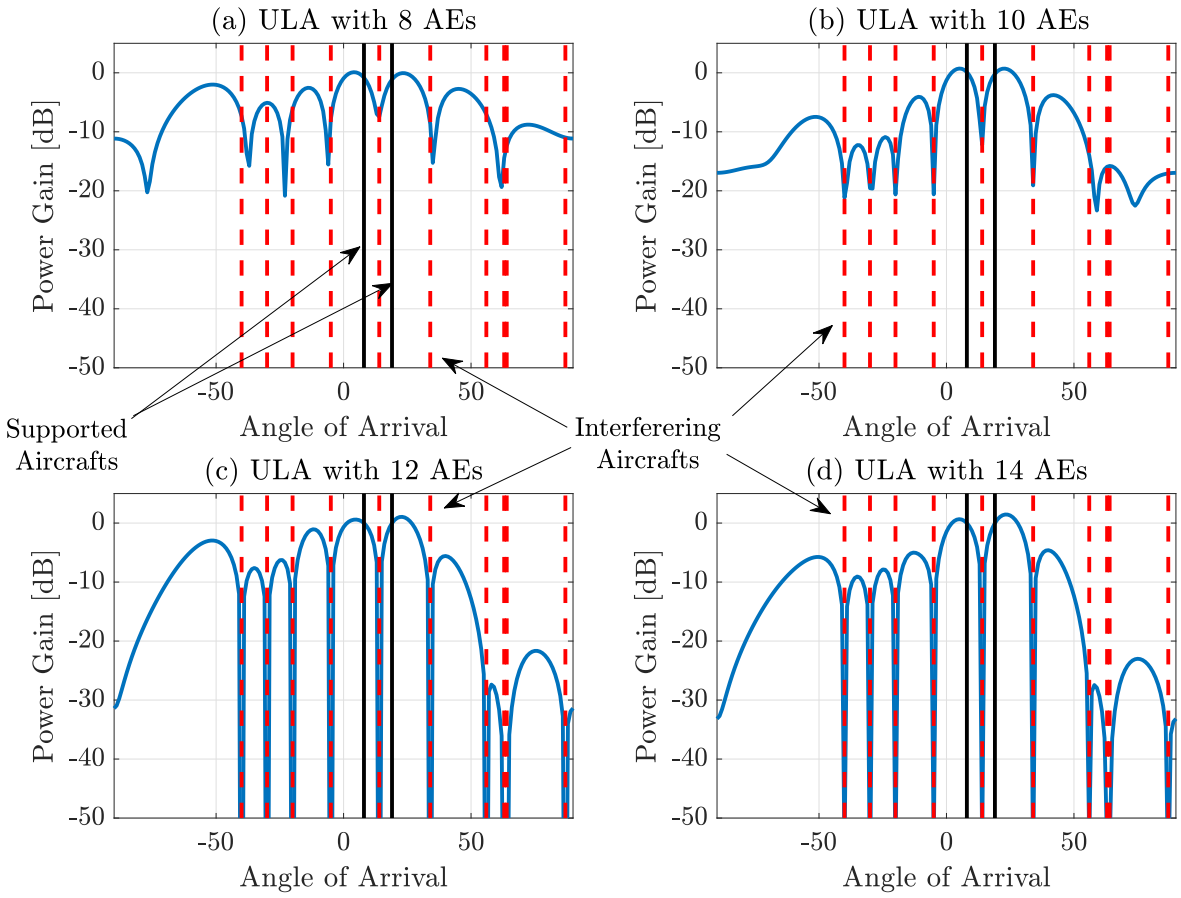

Fig. 3: The adaptive receive beamforming gain of a ULA equipped with a various number of AEs, when $U = 2$ aircraft are supported, while using the same time and frequency resources as $U_{intrf} = 10$ interfering aircraft.

C. Adaptive Receive Beamforming

An Adaptive Receive BeamFormer (ARBF) based on the Minimum Mean-Square Error (MMSE) criterion is employed at the GS, taking into consideration the angular position of the aircraft. More precisely, the ARBF tries to place "nulls" at the AoAs of the interfering aircraft, while receiving the signals of the supported aircraft unaltered. Rank-deficient scenarios, where there are more interfering aircraft than the number of AEs at a receive MFAA, may impose difficulties for the ARBF, since it will be unable to sufficiently attenuate the signal received from each interfering aircraft.

This is depicted in Fig. 3, where $U = 2$ supported aircraft transmit in the presence of $U_{intrf} = 10$ interfering aircraft relying on a Uniform Linear Array (ULA) having various number of AEs. In both Fig. 3a and Fig. 3b, we may observe that the ARBF is unable to uniformly attenuate the signals coming from an AoA, where interferers are positioned, since the ULA is equipped with fewer AEs than the total number of supported plus interfering users. In these situations, the ARBF tries to minimize the total interfering power, placing the nulls at specific AoAs, which are between the true AoAs of the interferers. Nonetheless, when $N_{r,AEs} = 10$ AEs are used, the attenuation becomes higher for the interefering aircraft, than for 8 AEs and no attenuation is imposed on the signals of the supported aircraft, compared to Fig. 3a. The minimum number of AEs $N_{r,AEs}$ that are required in the scenario of Fig. 3 in order to highly attenuate the interfering signals, while not affecting the supported aircraft' signals is equal to the total number of aircraft $N_{r,AEs} = U + U_{intrf} = 12$ AEs. The corresponding ARBF pattern is plotted in Fig. 3c, where we may observe that the interfering signals are attenuated by more than 50 dB. We have also shown the ARBF pattern, when more than 12 AEs are used in the receive AA. Explicitly, in Fig. 3d, there are $N_{r,AEs} = 14$ AEs at the ULA. The difference, compared to Fig. 3c is that we have more the side lobes, but interfering aircraft are attenuated more substantially. Hence, no performance difference is expected between the ARBF patterns of Fig. 3c and Fig. 3d.

A similar problem may also arise, when some of the interfering aircraft have an angular position close to the supported users, as illustrated in Fig. 1. This imposes a conflict on the ARBF, since it has to attenuate any interfering signal received at that AoA, but without attenuating any signal received at an AoA very close to that, since a supported aircraft has transmitted it.

As we will observe in Section IV, these two issues increase

the outage probability of the aeronautical system. In order to compensate for this, we have opted to separate the aircraft using orthogonal frequency or time resources, allowing only a specific subset of them to exploit the same resources. More specifically, we have introduced the notion of *angular vicinity* Φ of a supported user and the *maximum number of interfering aircraft in an angular vicinity* $U_{\max,AV}$. Based on these two values, a subset of aircraft is selected to use the same resources and hence to camp on the same NOMA resource. More precisely, every NOMA system is allowed to have a maximum of $U_{\max,AR}$ interfering aircraft in the angular vicinity Φ of each supported aircraft. Naturally, if possible, there should be no interfering aircraft in the vicinity of a supported aircraft. However, due to the high number of aircraft, this cannot always be guaranteed. In Fig. 4, we illustrate the opertation of the aforementioned parameters in the scenario of Fig. 1. Please note that the interfering aircraft that are outside of the supported aircraft' angular vicinity could be supported by the same resources and hence by our NOMA system, but the detection complexity required is expected to increase. Let us emphasize again that the interfering aircraft of a GS may be supported by a different GS.

Based on Fig. 3, the optimal angular vicinity for opting to allow an interfering stream to be processed by the iSD should depend on the antenna array employed for beamforming. In other words, it should optimally match the width of the beamformer's lobe aimed at the supported aircraft. However, a wide angular vicinity may be selected for improving the BER performance of the system, since it would take more interferers into consideration, especially those positioned at the peak of the beamforming pattern's side lobes.

The 2-dimensional A2G model of Fig. 1, which is considered in this paper may be extended to a 3-dimensional model. In that case, the angular vicinity will take the form of a right circular cone and the configurable parameter would be the opening angle of that cone. Similarly, the beamforming pattern of Fig. 3 would be 3-dimensional [49].

D. Receiver's System Model

After the signals have been received by the N_r AAs of the GS, the CP is removed and the Fast Fourier Transform (FFT) operation converts them to the frequency domain in order to allow further processing on a per subcarrier basis, as shown in Fig. 2. Therefore, we may model the transmission and reception processes in the frequency domain. More specifically, the received signals after the ARBF on the qth subcarrier may be modelled as

$$\mathbf{y}_q = \mathbf{W}_r \mathbf{H}_q \mathbf{x}_q + \mathbf{n}_q, \tag{1}$$

where $\mathbf{y}_q$ is the $(N_r \times 1)$-element vector that includes the signals received at each receive AA, $\mathbf{W}_r$ is the diagonal $(N_r \times N_r)$-element ARBF matrix, that includes the calculated beamforming coefficients based on both the AA's structure, as well as on the carrier frequency and on the AoA of each signal[1]. Furthermore, $\mathbf{H}_q$ is the $(N_r \times N_t \cdot U)$-element Frequency-Domain CHannel Transfer Function (FD-CHTF) matrix that includes the frequency-domain channel states experienced during the transmission, where N_t is the number of transmit AAs at the aircraft. The $(N_t \cdot U)$-element vector $\mathbf{x}_q$ includes the symbols transmitted by each transmit AA of each supported and interfering aircraft. Finally, still referring to (1), $\mathbf{n}_q$ is a $(N_r \times 1)$-element vector, which includes the Additive White Gaussian Noise (AWGN) samples, having a zero mean and a variance of N_0.

Then, the MUD of Fig. 2 detects the specific symbols that each of the supported aircraft transmitted with the aid of both the received signals and the *a priori* Log-Likelihood Ratios (LLR) obtained from the output of the channel decoders. The MUD outputs extrinsic LLRs for each of the supported aircraft' bits, which are then deinterleaved with the aid of the aircraft-specific deinterleavers. The DS despreader and the channel decoder of each supported aircraft exploit the deinterleaved extrinsic LLRs of the MUD as *a priori* LLRs, in order to estimate the transmitted information bits of each supported aircraft. If iterations are allowed between the MUD and the despreader/decoder (DES/DEC) processes, the outputs of the DES/DEC are then re-interleaved and fed back to the MUD. The MUD is configured to re-detect the transmitted symbols using the same received signals in combination with the updated *a priori* LLRs. After a predetermined number of MUD-DES/DEC iterations, a hard decision is performed at the output of the channel decoders in order to estimate the information bits of the supported aircraft.

E. Multi-User Detection

Let us now analyse the MUDs that will be employed as benchmarks in our performance simulations. More specifically, the optimal ML MUD and the conventional optimal depth-first HIHO SD [24], [27], [28] will be used for the scenarios, where hard-outputs are produced by the MUDs and there are no MUD-DES/DEC iterations. Additionally, the Max-Log-MAP MUD and the SISO single tree-search SD [30] will be used for comparison with our proposed SISO iSD, when MUD-DES/DEC iterations are allowed at the GS. For the sake of simplicity and without loss of generality, we omit the subscript q for the subcarriers, since the same operations are performed for each subcarrier of the system. Let us also define the effective channel $\mathbf{H}_{eff}$ as

$$\mathbf{H}_{eff} = \mathbf{W}_r \cdot \mathbf{H}, \tag{2}$$

which the transmitted symbol vector is subjected to, before it reaches the MUD.

1) Maximum-Likelihood MUD: The ML MUD searches through all legitimate multi-level symbols $\mathbf{x}$ for the specific multi-level symbol $\hat{\mathbf{x}}_{ML}$ that satisfies

$$\hat{\mathbf{x}}_{ML} = \arg\min_{\mathbf{x} \in \mathcal{M}^{N_t U}} \|\mathbf{y} - \mathbf{H}_{eff}\mathbf{x}\|^2, \tag{3}$$

[1]Each value in the diagonal of $\mathbf{W}_r$ is the inner product between the $(N_{r,AEs} \times 1)$-element beamforming vector of the AA, which is found based on the expected AoAs and the MMSE criterion, and an $(N_{r,AEs} \times 1)$-element vector, that includes the phase rotation of the signal received at each of the $N_{r,AEs}$ AEs of each receive AA.

where $\mathcal{M}$ is the size of the modulation scheme employed and may also be described as the set of all legitimate single-level symbols. Based on (3), the ML MUD finds the optimal multi-level symbol with respect to the MMSE criterion, but it has a complexity that increases exponentially with the number of supported aircraft and the number of bits per symbol, which may make it prohibitively complex in dense scenarios. Furthermore, since it does not take into consideration the *a priori* LLRs of the detected symbols, it is only suitable for non-iterative receivers.

2) Max-Log Maximum A posteriori Probability MUD: The Max-Log-MAP MUD exploits the *a priori* information that may have been obtained by previous MUD-DES/DEC iterations. Moreover, it outputs soft estimates of the detected symbols, in the form of extrinsic LLRs, making it more attractive than ML MUD even for non-iterative receivers, when the channel decoder accepts soft estimates as its input. The Max-Log-MAP MUD calculates the bit-based extrinsic LLRs of each supported aircraft's bits. It is based on the MAP MUD, which firstly calculates the *a posteriori* LLR of the uth aircraft's mth bit according to

$$L_{MUD,apo}^{MAP}\left(i_{u,m}\right) = \ln \frac{P\left(i_m^{(u)}=0\,|\,\mathbf{y}\right)}{P\left(i_m^{(u)}=1\,|\,\mathbf{y}\right)} = \ln \frac{\sum\limits_{\mathbf{x}\in\mathcal{X}_{u,m,0}} P\left(\mathbf{y}|\mathbf{x}\right)P\left(\mathbf{x}\right)}{\sum\limits_{\mathbf{x}\in\mathcal{X}_{u,m,1}} P\left(\mathbf{y}|\mathbf{x}\right)P\left(\mathbf{x}\right)}, \tag{4}$$

where $\mathcal{X}_{u,m,v}$ is the set of multi-level symbols, where the uth level's mth bit is equal to v, with $v \in \{0,1\}$, $P(\mathbf{x})$ is the *a priori* probability of transmitting $\mathbf{x}$ and the conditional probability $P(\mathbf{y}|\mathbf{x})$ is the channel probability of receiving $\mathbf{y}$ having transmitted $\mathbf{x}$, which is calculated based on

$$P(\mathbf{y}|\mathbf{x}) = \frac{1}{(\pi N_0)^{N_r}} \exp\left(-\frac{\|\mathbf{y}-\mathbf{H}_{eff}\mathbf{x}\|^2}{N_0}\right), \tag{5}$$

taking the random nature of the AWGN into consideration as well.

In (4), all legitimate multi-level symbols contribute to the calculation of the bit-based LLRs. The Max-Log MAP MUD allows us to estimate the optimal bit-based LLR value of (4), by performing the calculations in the log domain and selecting only the two specific multi-level symbols that maximize the numerator and the denominator of (4), respectively. In other words, the *a posteriori* LLR of the Max-Log-MAP MUD is calculated based on

$$L_{MUD,apo}\left(i_m^{(u)}\right) = \max_{\mathbf{x}\in\mathcal{X}_{u,m,0}}\left\{-\frac{\|\mathbf{y}-\mathbf{H}_{eff}\mathbf{x}\|^2}{N_0}+\ln P(\mathbf{x})\right\} - \max_{\mathbf{x}\in\mathcal{X}_{u,m,1}}\left\{-\frac{\|\mathbf{y}-\mathbf{H}_{eff}\mathbf{x}\|^2}{N_0}+\ln P(\mathbf{x})\right\}, \tag{6}$$

where we have used (4) and (5).

After the *a posteriori* LLR is calculated, the extrinsic LLR $L_{MUD,ex}$ is deinterleaved and fed to the DES/DEC of Fig. 2. The extrinsic LLR is calculated according to

$$L_{MUD,ex}\left(i_m^{(u)}\right) = L_{MUD,apo}\left(i_m^{(u)}\right) - L_{MUD,apr}\left(i_m^{(u)}\right), \tag{7}$$

where the *a priori* LLR $L_{MUD,apr}$ is found according to

$$L_{MUD,apr}\left(i_m^{(u)}\right) = \ln \frac{P\left(i_m^{(u)}=0\right)}{P\left(i_m^{(u)}=1\right)}. \tag{8}$$

3) Depth-First HIHO Sphere Decoder: The SD transforms the system of equations of (1) to an upper triangular system, which may be solved iteratively. The goal of the HIHO SD is to solve the same optimization problem as the ML MUD, which is stated in (3) and is copied here for convenience:

$$\hat{\mathbf{x}}_{SD}^{HIHO} = \arg\min_{\mathbf{x}\in\mathcal{M}^{N_tU}} \|\mathbf{y}-\mathbf{H}_{eff}\mathbf{x}\|^2. \tag{9}$$

Initially, we perform the QR-decomposition of the effective channel matrix $\mathbf{H}_{eff}$ as in

$$\mathbf{H}_{eff} = \mathbf{Q}\begin{bmatrix}\mathbf{R}\\ \mathbf{0}\end{bmatrix}, \tag{10}$$

where $\mathbf{Q} = [\mathbf{Q}_1\ \mathbf{Q}_2]$ is an $(N_r \times N_r)$-element orthogonal matrix with $\mathbf{Q}_1$ and $\mathbf{Q}_2$ being $(N_r \times N_t \cdot U)$-element and $(N_r \times N_r - N_t \cdot U)$-element matrices, respectively, $\mathbf{R}$ is an $(N_r \times N_t \cdot U)$-element upper triangular matrix and $\mathbf{0}$ is a $(N_r - N_t \cdot U \times N_t \cdot U)$-element all-zero matrix. Please note that (10) is valid for the specific scenarios, where $N_r \geq N_t \cdot U$. By multiplying the right-hand side of (9) by $\mathbf{Q}^H$, we obtain

$$\begin{aligned}\hat{\mathbf{x}}_{SD}^{HIHO} &= \arg\min_{\mathbf{x}\in\mathcal{M}^{N_tU}} \left\|\mathbf{Q}^H\mathbf{y}-\mathbf{Q}^H\mathbf{H}_{eff}\mathbf{x}\right\|^2\\ &= \arg\min_{\mathbf{x}\in\mathcal{M}^{N_tU}} \left\{\left\|\mathbf{Q}_1^H\mathbf{y}-\mathbf{R}\mathbf{x}\right\|^2 + \|\mathbf{Q}_2\mathbf{y}\|^2\right\}\\ &= \arg\min_{\mathbf{x}\in\mathcal{M}^{N_tU}} \|\tilde{\mathbf{y}}-\mathbf{R}\mathbf{x}\|^2,\end{aligned} \tag{11}$$

where $\|\mathbf{Q}_2\mathbf{y}\|^2$ was omitted, since it is always positive and it does not depend on $\mathbf{x}$, while $\tilde{\mathbf{y}} = \mathbf{Q}_1^H\mathbf{y}$. By exploiting the fact that $\mathbf{R}$ is an upper triangular matrix, we obtain

$$\hat{\mathbf{x}}_{SD}^{HIHO} = \arg\min_{\mathbf{x}\in\mathcal{M}^{N_tU}} \sum_{i=1}^{N_tU}\left|\tilde{y}_i - \sum_{j=i}^{N_tU} R_{i,j}x_j\right|^2, \tag{12}$$

where $\tilde{y}_i$ is the ith element of the vector $\tilde{\mathbf{y}}$, $R_{i,j}$ is the element in the ith row and jth column of $\mathbf{R}$ and x_j is the jth element of the vector $\mathbf{x}$.

The depth-first HIHO SD solves the minimization problem of (12) using a tree search, as illustrated in Fig. 5 for $U = 3$ supported aircraft equipped with $N_t = 1$ AA each and employing the QPSK modulation scheme. Starting from the $N_tU = 3$rd level, the SD finds the legitimate single-level symbol x_{N_tU} that minimizes

$$\check{x}_{N_tU} = \arg\min_{x\in\mathcal{M}} |\tilde{y}_{N_tU} - R_{N_tU,N_tU}x_{N_tU}|^2, \tag{13}$$

as well as the associated distance between the received signal that corresponds to that level y_{N_tU} and the noiseless recon-

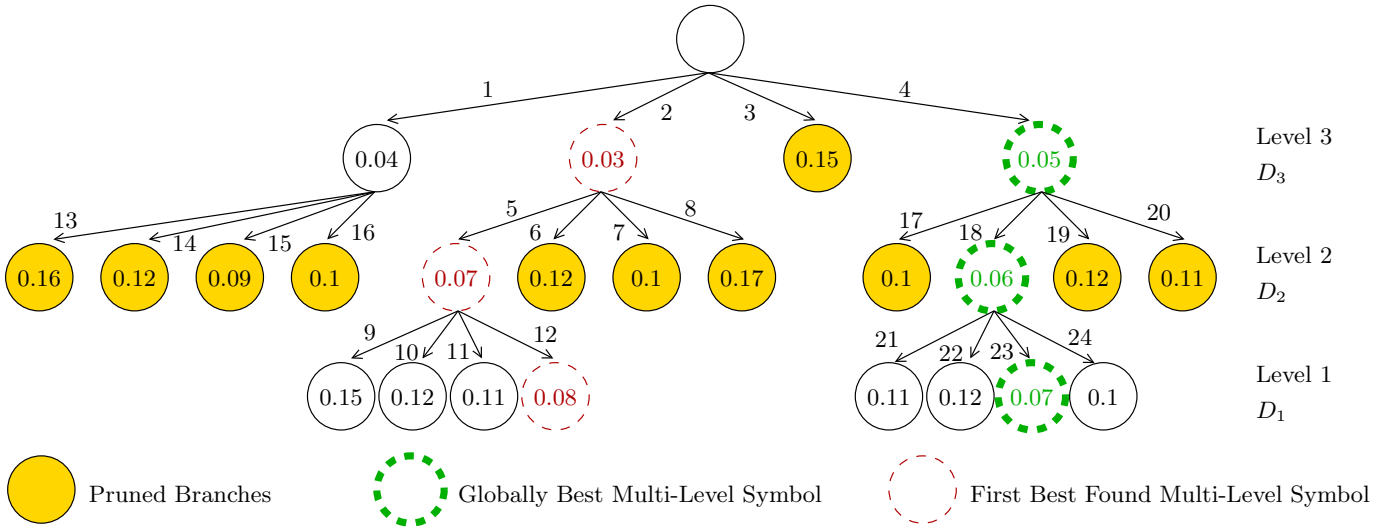

Fig. 5: The HIHO SD's operation in an example scenario, where there are $U = 3$ supported users with $N_t = 1$ MFAA each using the QPSK modulation scheme. The numbers next to the arrows denote the order in which the nodes are visited. The numbers in the nodes state the accumulative distance metric of the so-far built multi-level symbol. The HIHO SD aims to find the multi-level symbol that corresponds to the minimum distance metric D_1. All nodes presented are visited by the HIHO SD (24 out of the total 84 legitimate nodes).

structed single-level symbol, as in

$$D_{N_tU} = |\tilde{y}_{N_tU} - R_{N_tU,N_tU}\check{x}_{N_tU}|^2 . \tag{14}$$

Having selected the best symbol from the last level, the same procedure is applied for the previous levels until a symbol has been selected from each level, while updating the distance metric D_i. More specifically, for the ith level, the distance metric is updated as in

$$D_i = \sum_{l=i}^{N_tU} \left| \tilde{y}_l - \sum_{j=l}^{N_tU} R_{l,j}\check{x}_j \right|^2 , \tag{15}$$

where the already chosen single-level symbols of the subsequent level contribute to it. We may observe that according to (15), D_1 corresponds to the metric described in (12). Therefore, the goal of the SD is to find the specific route in the search tree of Fig. 5, that is associated with the minimum D_1.

After finding an initial legitimate multi-level symbol and its associated distance metric $D_1(\hat{\mathbf{x}})$, the depth-first HIHO SD proceeds to the immediately subsequent stage 2 and searches for another path in the tree, for which the distance metric D_2 satisfies $D_2(\check{\mathbf{x}}) < D_1(\hat{\mathbf{x}})$, since that would mean that the new path has the potential to result in a lower $D_1(\check{\mathbf{x}})$ value than the current one $D_1(\hat{\mathbf{x}})$. From another point of view, the SD *prunes* the branches for which $D_2(\check{\mathbf{x}}) \geq D_1(\hat{\mathbf{x}})$, since it is impossible for those branches to result in a lower distance metric than $D_1(\hat{\mathbf{x}})$, due to the fact that a non-negative value is added to the distance metric at each level, as encapsulated in

$$D_i = D_{i+1} + \left| \tilde{y}_i - \sum_{j=i}^{N_tU} R_{i,j}\check{x}_j \right|^2 . \tag{16}$$

Therefore, the HIHO SD moves up and down the tree, pruning branches that have no potential of leading to a better solution, while visiting branches that may lead to an improved estimate. Naturally, the HIHO SD terminates, when there is no available branch left to visit and it outputs the multi-level symbol $\hat{\mathbf{x}}$ that led to the minimum distance metric $D_1(\hat{\mathbf{x}})$.

4) Depth-First SISO Single Tree Search Sphere Decoder: The depth-first SISO SD follows the same tree search as the HIHO SD of Section II-E3, apart from two main differences. Firstly, the distance metric now takes into consideration both the noise power and the *a priori* probability of each level's symbol's bits, since a soft estimate has to be calculated by the SD. Secondly, the SISO SD follows the Max-Log approach of the Max-Log-MAP MUD, hence it has to find the specific multi-level symbols that maximize the numerator and the denominator of the bit-based LLRs of the current multi-level symbol, as illustrated in Fig. 6. Please note that the globally optimal multi-level symbol, which is found using the approach of the HIHO SD of Section II-E3, will be the multi-level symbol that maximizes either the numerator or the denominator of each of the multi-level symbol's bits, as shown in Fig. 6. Therefore, the SISO SD has to find both this symbol, as well as at most $\log_2(M^{N_tU})$ multi-level symbols, where M is the constellation size of the modulation scheme.

The distance metric in the depth-first SISO SD is calculated according to

$$D_i^{SISO} = \sum_{l=i}^{N_tU} \left(\frac{1}{N_0} \left| \tilde{y}_l - \sum_{j=l}^{N_tU} R_{l,j}\check{x}_j \right|^2 - \ln P_a\left(\check{\mathbf{x}}^{(i)}\right) \right) , \tag{17}$$

where $P_a\left(\check{\mathbf{x}}^{(i)}\right)$ takes into account the previous choices of the

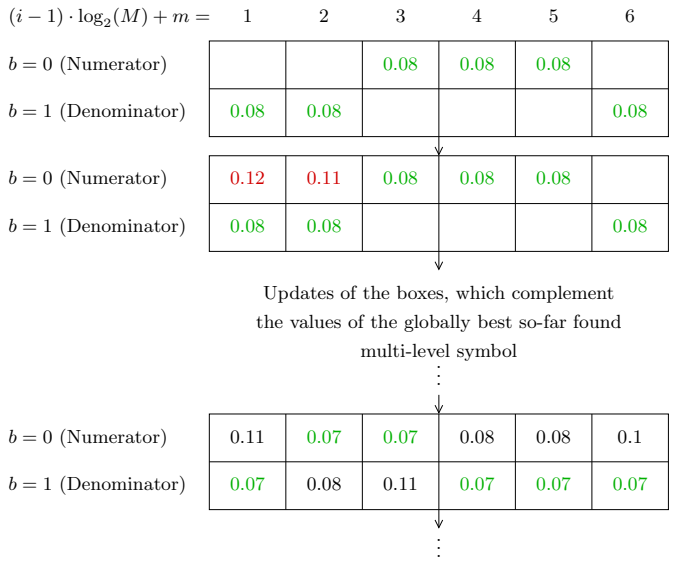

Fig. 6: The operation of the SISO SD, where the minimum distance metric for the numerator and the denominator of each bit of the multi-level symbol has to be found. For terms of clarity, we have opted to use the same values as in Fig. 5 for the distance metrics D_1 of the SISO scenario. The only difference to the HIHO scenario of Fig. 5 is that in the SISO scenario, the left-most pruned branches are now visited, since they lead to a lower D_1 value for some of the complementary boxes (0.11). The distance metric D_1 of the globally best so-far-found multi-level symbol is denoted by the green color, while we use red color to indicate the updated values of a "box".

SD, as in

$$P_a\left(\check{\mathbf{x}}^{(i)}\right)=\prod_{i=i}^{N_tU}P\left(\check{x}_i|\check{\mathbf{x}}^{(i+1)}\right). \tag{18}$$

The term of $-\ln P_a\left(\check{\mathbf{x}}^{(i)}\right)$ in (17) may be approximated as [30]

$$-\ln P_a\left(\check{\mathbf{x}}^{(i)}\right)\approx\sum_{m=1}^{M}\frac{1}{2}\left(\left|L_{i,m}^{apr}\right|-\check{s}_{i,m}L_{i,m}^{apr}\right), \tag{19}$$

where $\check{s}_{i,m}=+1$ if $\check{b}_{i,m}=0$ and $\check{s}_{i,m}=-1$ if $\check{b}_{i,m}=1$, while $L_{i,m}^{apr}$ is the *a priori* LLR of the ith level's mth bit, that is obtained by the output of the DES/DEC operation. Therefore, the update of the distance metric is performed according to

$$D_i^{SISO}=D_{i+1}^{SISO}+\frac{1}{N_0}\left|\tilde{y}_i-\sum_{j=i}^{N_tU}R_{i,j}\check{x}_j\right|^2+\sum_{m=1}^{M}\frac{1}{2}\left(\left|L_{i,m}^{apr}\right|-\check{s}_{i,m}L_{i,m}^{apr}\right). \tag{20}$$

Let us denote by $\hat{\mathbf{x}}$ the multi-level symbol that corresponds to the globally minimum D_1 metric and by $\hat{\mathbf{x}}_{i,m}^{compl}$ we denote the multi-level symbol that has the minimum D_1 for the complementary box of the ith level's mth bit in Fig. 6. The extrinsic LLR calculation of the ith level's mth bit $L_{i,m}^{ex}$ is then performed based on

$$L_{i,m}^{ex}=\begin{cases}d\left(\hat{\mathbf{x}}_{i,m}^{compl}\right)-D_1\left(\hat{\mathbf{x}}\right), & \hat{b}_{i,m}=0\\ D_1\left(\hat{\mathbf{x}}\right)-d\left(\hat{\mathbf{x}}_{i,m}^{compl}\right), & \hat{b}_{i,m}=1\end{cases}, \tag{21}$$

where we have

$$d\left(\hat{\mathbf{x}}_{i,m}^{compl}\right)=\begin{cases}D_1\left(\hat{\mathbf{x}}_{i,m}^{compl}\right)-L_{i,m}^{apr}, & \hat{b}_{i,m}=0\\ D_1\left(\hat{\mathbf{x}}_{i,m}^{compl}\right)+L_{i,m}^{apr}, & \hat{b}_{i,m}=1\end{cases}. \tag{22}$$

Therefore, the depth-first single tree search SISO SD aims for filling the boxes of Fig. 6 with the multi-level symbols that have the minimum distance metric D_1. In order to do so, the tree search commences by finding an initial multi-level symbol solution, similarly to the HIHO SD case. When it does, it updates the corresponding boxes with its associated distance metric D_1. The difference with respect to the search procedure, when compared to the HIHO SD of Section II-E3 manifests itself in the specific methodology followed during moving up and down the tree for making a decision to either ignore or visit a branch. That decision is taken based on whether the candidate branch has the potential to lead to a multi-level symbol that may be associated with a lower distance metric D_1 or $D_1(\check{\mathbf{x}}_{j,m}^{compl})$, with $j=i,\ldots,N_tU$. In other words, the SISO SD will only visit a branch, if it is possible to find a multi-level symbol that may further reduce the distance metric of a box complementary to the box occupied by the up-to-date globally best found symbol, for any of the previously visited levels' bits. If that branch actually leads to a multi-level symbol that has a lower D_1 value than the globally best symbol, then $\hat{\mathbf{x}}$ and $D_1(\hat{\mathbf{x}})$ are updated with the new values, while the previous D_1 values automatically become the best values found for the now complementary boxes. This process guarantees that the best multi-level symbols are found. However, the search complexity is higher than that of the HIHO SD of Section II-E3, since more nodes are visited on average.

III. Interference-Exploiting Sphere Decoder

The iSD takes into account the fact that the received signal is contaminated by interference and it treats it as "structured noise". In this section we describe its operation in both HIHO and SISO scenarios.

A. HIHO iSD

The HIHO iSD operates in a very similar manner to the HIHO SD, as far as the supported users are concerned. The supported users' symbols occupy the first N_tU levels of the HIHO iSD, as illustrated in Fig. 7, in exactly the same way as the conventional HIHO SD. The HIHO iSD includes additional levels, which correspond to the specific interferers, whose received signal power is above the thermal noise's power. The thermal noise's power N_0, which is modelled as AWGN in (1), depends on the bandwidth. The received signal strength of the interferers substantially depends on the signal's AoA, since an adaptive beamformer is employed, as well as on the distance between the interfering aircraft and the GS. Therefore, even if there are multiple interfering aircraft operating simultaneously

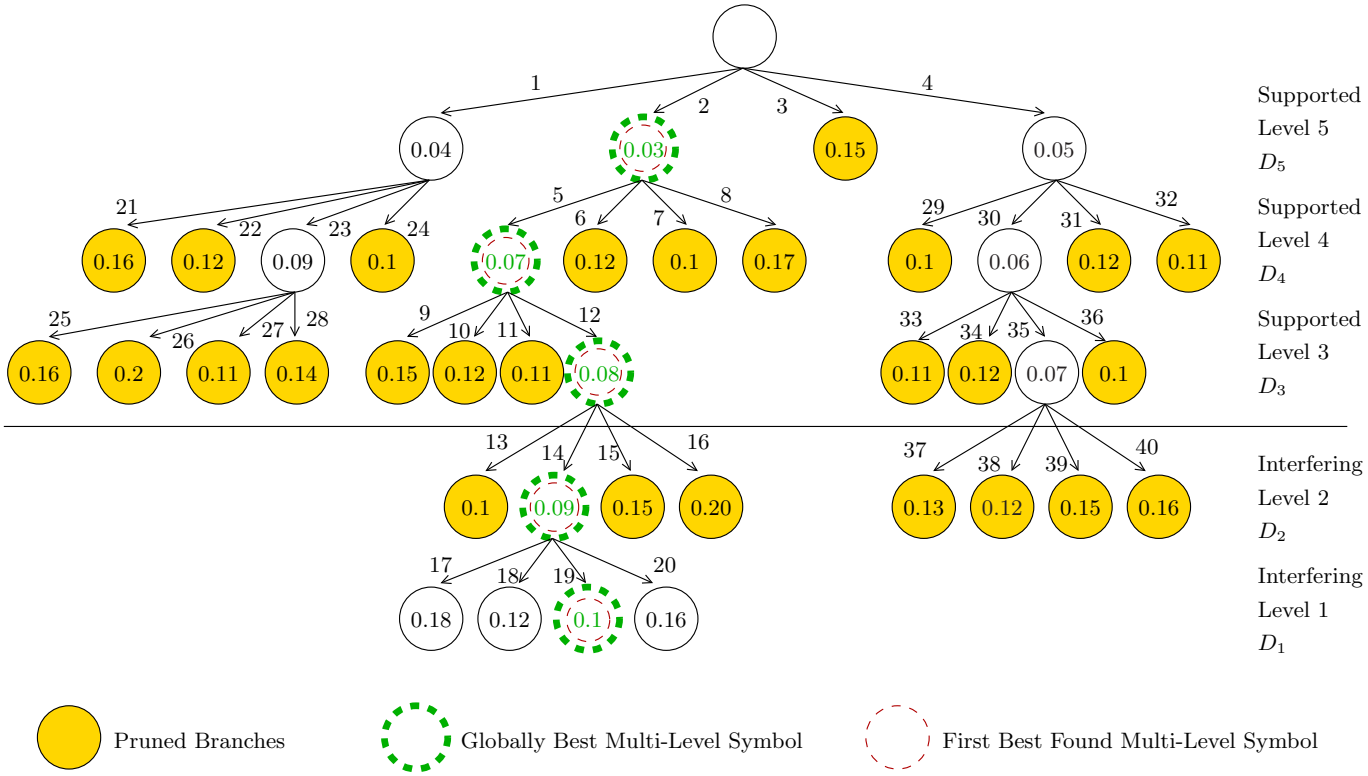

Fig. 7: The HIHO iSD's operation in an example scenario, where there are $U = 3$ supported users with $N_t = 1$ MFAA each using the QPSK modulation scheme and $L_{intrf} = 2$ interfering levels. The numbers next to the arrows denote the order in which the nodes are visited. The numbers in the nodes state the accumulative distance metric of the so-far built multi-level symbol. The HIHO SD aims to find the multi-level symbol that corresponds to the minimum distance metric D_1. All nodes presented are visited by the HIHO iSD (40 out of the total 84 legitimate nodes that the ML MUD would visit).

over the same resources as the supported aircraft, there is a high probability that none of their interfering signals will be stronger than the thermal noise. Hence, there is no need to include their signals in the detection process, since the random AWGN will dominate the "structured noise" of the interferers. On the other hand, in the cases, where the interfering signals have a higher power than that of the thermal noise, we may exploit them in order to improve the detection estimates.

The HIHO iSD actively exploits the interfering signals that are deemed to be sufficiently strong, by including them in the detection process, as depicted in Fig. 5 for two interferers. Please note that since the aim of the HIHO iSD is not to detect the symbols of the interferers, but only those of the supported users, the number of interfering levels in the HIHO iSD may be different from the number of interfering signals above the noise level. For example, if three interferers' signals managed to pass through the beamformer and have a higher power than the noise level, the HIHO iSD may use all three of them as three additional levels, or it may only use the strongest of the three signals as a single additional level. As expected, there is a trade-off between the performance improvement attained and the associated additional complexity imposed by adding more levels in a sphere decoder. Furthermore, whether there are any interfering levels in the iSD or none at all, heavily depends on the specific scenario, including the signals' AoAs. Therefore, in our evaluation process, we define $L_{intrf}^{\max}$ as the maximum affordable number of interfering levels in the iSD. For example, in Fig. 7 we have $L_{intrf}^{\max} = 2$ and we have no information on how many interfering signals have a higher power than the thermal noise's power. However, we know that the two included interfering levels represent the two strongest interfering signals received. This is estimated based on both the AoA of the interfering signals, as well as on their distance and transmission power.

As in the conventional SDs, the levels supported in the SD are sorted so that the top level belongs to the strongest user. This reduces the complexity of the SD, since there is a higher probability that both the SD and the iSD will make the correct decision early in the tree search, allowing them to prune a more substantial part of the unexplored tree later in the search. We have opted for using the same methodology for the $L_{intrf}^{\max}$ interfering levels in the iSD, sorting the interfering levels from the strongest to the weakest. The distance metric for the iSD remains the same for each level, but since more levels may be added, it becomes

$$D_i = \sum_{l=i}^{N_t\cdot(U+L_{intrf})} \left| \tilde{y}_l - \sum_{j=l}^{N_t\cdot(U+L_{intrf})} R_{l,j}\check{x}_j \right|^2, \qquad (23)$$

where $L_{intrf} \in \{0, 1, \ldots, L_{intrf}^{\max}\}$ is the number of interfering levels at a specific time slot, which cannot be higher than $L_{intrf}^{\max}$. The recursive calculation of D_i on the ith level of the

iSD is performed based on

$$D_i = D_{i+1} + \left| \tilde{y}_i - \sum_{j=i}^{N_t \cdot (U+L_{intrf})} R_{i,j} \check{x}_j \right|^2 . \quad (24)$$

Since in a non-iterative receiver only the most likely multi-level symbol is required by the MUD, when the iSD concludes its search, only the symbols of each supported level are passed to the decoders.

Upon comparing the HIHO iSD of Fig. 7 to the HIHO SD of Fig. 5, we may observe that they end up with different final solutions for the search problem. Since the HIHO iSD exploits the two strongest interfering signals, it is expected to be a more accurate estimate, even if its partial distance metric D_3 is higher than the D_1 metric found by the HIHO SD in Fig. 5. However, a higher complexity is imposed, since the HIHO iSD in Fig. 7 visits 40 nodes, while the HIHO SD of Fig. 5 only visits 24 nodes.

The complexity of the HIHO iSD is always expected to be higher than that of the conventional SD, since in the former we include more levels in the tree search. The complexity increase depends on the selected value for $L_{intrf}^{\max}$. Compared to the ML MUD, the HIHO iSD is expected to exhibit a lower complexity, when $L_{intrf}^{\max}$ is kept low, provided that the SIR is high enough.

B. SISO iSD

The proposed depth-first SISO iSD also has similarities to the depth-first SISO SD of Section II-E4. Firstly, since only the bit-based LLRs of the supported aircraft' symbols are fed to the DES/DEC operation of Fig. 2, there is no need to caclulate the LLRs of the interfering aircraft' bits. Therefore, the memory blocks of the LLR boxes have exactly the same size and the same number as for the SISO SD, which are shown in Fig. 6. The difference between the SISO iSD and the SISO SD is in the specific values that enter the numerator and the denominator of each LLR expression.

Since the LLR of a bit, which belongs to a multi-level symbol, depends on the *a priori* probability of the rest of the bits that form that same multi-level symbol, we have opted for excluding the distance metrics, and hence not including the corresponding bits, of the interfering levels in the calculation of either the numerator or of the denominator of the supported bits' LLRs. In other words, the distance metric that contributes to the calculation of the LLRs is that of the lowest level of the supported levels. For example, in Fig. 7, it would be D_3. This changes the calculation of the extrinsic LLRs in the SISO iSD to

$$L_{i,m}^{ex} = \begin{cases} d\left(\hat{\mathbf{x}}_{i,m}^{compl}\right) - D_{1+L_{intrf}}\left(\hat{\mathbf{x}}\right), & \hat{b}_{i,m} = 0 \\ D_{1+L_{intrf}}\left(\hat{\mathbf{x}}\right) - d\left(\hat{\mathbf{x}}_{i,m}^{compl}\right), & \hat{b}_{i,m} = 1 \end{cases} , \quad (25)$$

where we have

$$d\left(\hat{\mathbf{x}}_{i,m}^{compl}\right) = \begin{cases} D_{1+L_{intrf}}\left(\hat{\mathbf{x}}_{i,m}^{compl}\right) - L_{i,m}^{apr}, & \hat{b}_{i,m} = 0 \\ D_{1+L_{intrf}}\left(\hat{\mathbf{x}}_{i,m}^{compl}\right) + L_{i,m}^{apr}, & \hat{b}_{i,m} = 1 \end{cases} \quad (26)$$

for $i = L_{intrf}+1, L_{intrf}+2, \ldots, N_t \cdot U$. The calculation of each level's distance metric may be carried out recursively as in

$$D_i^{SISO} = D_{i+1}^{SISO} + \frac{1}{N_0} \left| \tilde{y}_i - \sum_{j=i}^{N_t(U+L_{intrf})} R_{i,j} \check{x}_j \right|^2 + \begin{cases} \sum_{m=1}^{M} \frac{1}{2}\left(\left| L_{i,m}^{apr} \right| - \check{s}_{i,m} L_{i,m}^{apr} \right) & i > L_{intrf} \\ 0 & i \leq L_{intrf} \end{cases} , \quad (27)$$

where we have made it explicit that it is not fruitful to calculate the third term of (27), when searching at the interfering levels, since the associated *a priori* LLRs of the interfering bits will always be equal to 0, due to the fact that they are not included in the decoding iterations.

The effect of including interfering levels in the iterative SISO iSD is in the search for $\mathbf{x}$ and $\mathbf{x}_{i,m}^{compl}$, which determine the specific multi-level symbols whose partial distance metric will be entered in the LLR boxes of Fig. 6. Our approach is based on the fact that the zero-valued *a priori* LLR values of the interfering bits will not have been updated, even if we allow iterations at the receivers, since their bit stream will not be decoded. Hence, we wanted to limit any bias that this would impose on the detection process, by limiting their operation to choosing the "best" multi-level symbols, without contributing more substantially to the LLR calculation. The search for the best multi-level symbols that fill the numerator and the denominator boxes in Fig. 6 is carried out in the same way as for the SISO iSD, comparing the D_1 distance metrics in order to determine, which particular symbol should contribute to the max-log LLRs. Additionally, there are interfering levels as in the HIHO iSD, increasing the complexity imposed, when compared to the SISO iSD.

In conclusion, the SISO iSD initially finds the best multi-level symbols for the numerators and denominators of each supported bit's LLR based on their total distance metric D_1, which includes the contribution of the interfering levels, as in Fig. 7. Having found these symbols, the LLR calculation is performed with the aid of the partial distance metric $D_{1+L_{intrf}}$, which only includes the contributions of only the supported aircraft' bits. Again, the bit-based *a priori* probabilities that contribute to the calculation of the extrinsic LLRs only belong to the supported aircraft' bits. The fact that the specific multi-level symbols that contribute to the calculation of the max-log LLR are different for the SISO iSD and for the Max-Log-MAP MUD and for the SISO SD will result in different LLR values.

IV. Simulation Results

Let us now focus our attention on evaluating an A2G system, where $U = 2$ aircraft are supported by the GS using an MC-IDMA NOMA system, where a variable number of interferers is also using the same resources. We have opted for a carrier frequency of $f_c = 11$ GHz and a maximum relative velocity of $\mathrm{v}_{\max} = 440$ m/s [46]. Furthermore, the GS is equipped with $N_r = 4$ AAs with $N_{r,AEs} = 10$ AEs each,

TABLE II: Default Parameters of the Investigated Scenarios

No. of Supported aircraft	$U = 2$
No. of Interfering aircraft	$U_{intrf} = 15$
No. of AAs at each Aircraft	$N_t = 1$
No. of AAs at Ground Station	$N_r = 4$
No. of antenna elements at each AA	$N^t_{AA} = 1$
	$N^r_{AA} = 10$
Spreading Factor	$SF = 2$
Channel Model	A2G Multipath Channel [46]
Max. Relative Velocity	$v = 440$ m/s
Carrier Frequency	$f_c = 11$ GHz
AE Spacing	$\lambda/2 = 1.36$ cm
Sampling Frequency	$f_s = 15.36$ MHz
No. of Subcarriers	$\mathcal{Q} = 1024$
Cyclic Prefix	CP = 103 samples
Subcarrier Spacing	15 kHz
Modulation Scheme	QPSK
Channel Code	RSC with $R = 1/2$
	8 Trellis states
Frame Length	7168 information bits per aircraft
Average K_{rice} factor	15 dB
Angular Vicinity	$\Phi = 10^\circ$

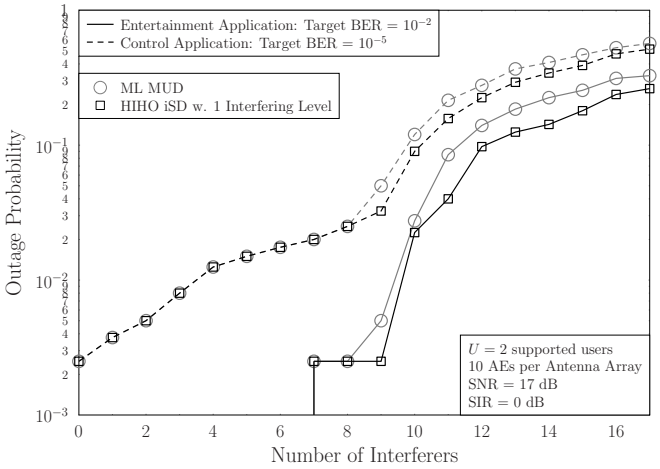

Fig. 8: Outage probability when $U = 2$ supported users operate in a system with a various number of non-orthogonal interferers for both entertainment and control applications at SNR = 17 dB and SIR = 0 dB. The ML MUD and the proposed HIHO iSD with $L_{intrf} = 1$ interfering level are used for detection. The rest of the parameters are gathered in Table II.

while the aircraft are assumed to transmit using $N_t = 1$ AA and $N_{t,AEs} = 1$ AE each, essentially precluding the employment of transmit precoding and beamforming, in order to focus our attention on the evaluation of the adaptive receive beamforming and detection method. Each aircraft transmits 14 OFDM symbols per packet, with $\mathcal{Q} = 1024$ subcarriers per OFDM symbol and a $QPSK$ symbol on each subcarrier. As a channel code we have used a Recursive Systematic Convolutional (RSC) code having a rate of $R = 1/2$ and 8 Trellis states, while the spreading factor of the IDMA system is chosen to be SF = 2. The default parameters of the simulated systems are gathered in Table II.

In Fig. 8, there is a variable number of interfering users, who use the same resources as the two supported users. Moreover, there is no orthogonal separation of the users based on their AoA, because we wanted to show the detrimental effects that many interferers may cause, if their AoA is similar to that of the supported users. In other words, the A2G scenario characterized in Fig. 8 is that of Fig. 1. We have estimated the outage probability for a high-integrity control application, where the target BER is 10^{-5}, and for an entertainment application, where the associated target BER is 10^{-2}. These BERs were satisfied at an SNR value of 17 dB and an SIR value of 0 dB, respectively. An outage event is declared, when the instantaneous BER of the investigated application is above the target BER of that specific application. Both the optimal ML MUD and the proposed HIHO iSD have been employed in order to compare their performance. We may observe that when up to $U_{intrf} = 8$ interfering aircraft are present, the performance of the two detectors is the same. The reason for this trend is that the receive AAs have $N_{r,AEs} = 10$ AEs each, therefore the adaptive beamformer is capable of mitigating the interfering signals. This essentially converts the HIHO iSD to the conventional HIHO SD, since the interfering signals will not be strong enough to become additional interfering levels in the HIHO iSD. When there are more than $N_{intrf} = 8$ interferers in Fig. 8, the beamformer becomes unable to sufficiently mitigate them, hence we observe a difference in the outage probability trends. The HIHO iSD performs in these cases better than the ML MUD, since it exploits the strongest interfering signals. However, the outage probability is still high, suggesting for us to proceed by separating a subset of the users orthogonally, similarly to Fig. 4.

From this point onwards, the A2G systems considered include both supported and interfering users, who rely on the same resources, as well as supported and interfering users, who use orthogonal resources, where the separation has been determined by the angular vicinity Φ and by the maximum number of interfering aircraft $U_{\max,AV}$ in the angular vicinity. More specifically, $U = 2$ supported aircraft and $U_{intrf} = 15$ interfering aircraft use the same resources, with $\Phi = 10^\circ$ and $U_{\max,AV} = 1$, unless specified differently in a figure.

In Fig. 9 we illustrate the BER performance of the system, when the $U = 2$ supported users are outside each other's angular vicinity of $\Phi = 10^\circ$. This would force the adaptive receive beamformer not only to try to attenuate the signals of the $U_{intrf} = 15$ interferers using $N_{r,AEs} = 10$ AEs, but also to create two separate main lobes in the direction of the pair of supported users. We may observe that by using the HIHO iSD associated with a single interfering level we achieve a gain in terms of both the SNR required and the SIR tolerated. For example, assuming a target BER of 10^{-5}, there is an SIR gain of 2.5 dB, when operating at an SNR of 23 dB. Similarly, the HIHO iSD requires an SNR of 19 dB in order to achieve the same performance, when we have SIR = 5 dB, while the

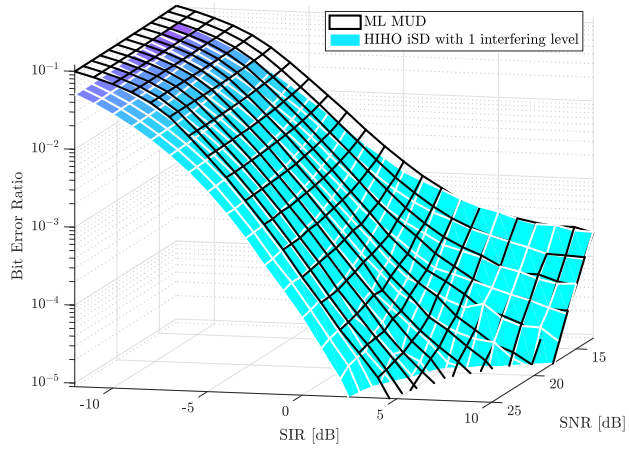

Fig. 9: BER performance with respect to SNR and SIR, when $U = 2$ supported and $U = 15$ interfering aircraft transmit using the same resources. The $U = 2$ users are outside each other's angular vicinity of $\Phi = 10^{\circ}$ and there is maximum $U_{\max,AV} = 1$ interferer in each user's angular vicinity. The rest of the parameters are gathered in Table II.

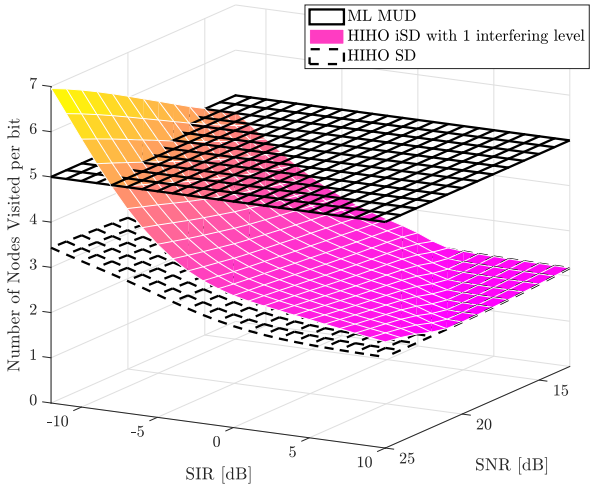

Fig. 10: Number of nodes visited per bit with respect to SNR and SIR, when $U = 2$ supported and $U = 15$ interfering aircraft transmit using the same resources. The $U = 2$ users are outside each other's angular vicinity of $\Phi = 10^{\circ}$ and there is maximum $U_{\max,AV} = 1$ interferer in each user's angular vicinity. The rest of the parameters are gathered in Table II.

ML MUD requires an SNR of 23 dB.

In the high-SIR, low-SNR region of Fig. 9, we may observe that the two detectors have a similar performance. This was expected, since at high SIR and low SNR values, the interferers' signals are well below the noise level, causing the HIHO iSD to behave as the conventional depth-first HIHO SD, which achieves the optimal performance of the ML MUD. As the SNR increases for a given SIR value, the strength of the interfering signals is also increased. Therefore, the HIHO iSD becomes prone to including an interfering level more often for higher SNR values, hence resulting in an improved performance compared to the ML MUD. Naturally, the same applies for low-SIR values, since the interfering signals' strength is high in that region. Indeed, based on Fig. 9, for low SIR values the HIHO iSD always outperforms the ML MUD, but the overall BER performance remains inadequate for high-integrity services.

Figure 10 depicts the number of nodes visited by the search algorithm employed, normalized with respect to the number of bits per multi-level symbol of the supported users. As mentioned in Section III, the HIHO iSD has a higher complexity than the conventional HIHO SD, when interfering levels are included in the tree search. This occurs when the interfering signals' strength is sufficiently high. In the low-SIR, high-SNR region this happens quite often, since the Interference-to-Noise Ratio (INR) is very high. In fact, the additional interfering levels of the HIHO iSD appear so often, that the complexity becomes higher than that of the ML MUD. However, this is associated with a high BER, as we may observe in Fig. 9, therefore it does not constitute part of our desired operating region. At the high-SIR, low-SNR region, the behaviour is the opposite, since the SINR is so low, that the HIHO iSD behaves exactly as the HIHO SD in terms of its BER vs complexity performance. Following the same trend as the HIHO SD, the complexity of the HIHO iSD is reduced, when the SIR is increased. This is due to the fact that the probability of visiting the globally best nodes of the tree search becomes higher, when the SIR is higher in an interference-limited system. By observing both Fig. 9 and Fig. 10, we may conclude that the proposed HIHO iSD outperforms both the ML MUD, and hence the depth-first HIHO SD, despite its lower complexity than that of the ML MUD, but higher than that of the HIHO SD.

If the GS supports $U = 2$ aircraft, which are angularly close to each other, the performance is expected to be improved for both the HIHO iSD and the ML MUD, since the adaptive beamformer will have to have a single main lobe, focusing the rest of its resources on mitigating the interfering signals. This is verified in Fig. 11, where the same system is simulated as in Fig. 9, apart from the difference that the $U = 2$ supported aircraft are angularly close to each other. We may observe similar trends for the ML MUD as in Fig. 9, while having an SIR-gain of approximately 2.5. The HIHO iSD associated with $L_{intrf}^{\max} = 1$ performs much better when the AoAs supported are similar, as seen in Fig. 11, compared to when the supported AoAs are very different from each other, as in Fig. 9, because in Fig. 11 there are fewer interferers, which have a sufficiently high power. The strongest of those interferers is taken into account by the HIHO iSD, hence resulting in an improved performance in Fig. 11, when compared to not only the ML MUD, but also to the HIHO iSD in the scenario of Fig. 9, where the supported aircraft have different AoAs.

In Fig. 12 we investigate the effect that multiple interfering levels have on the performance of the HIHO iSD, for various values of angular vicinity Φ, when the maximum number of interferers in the angular vicinity of the supported users is

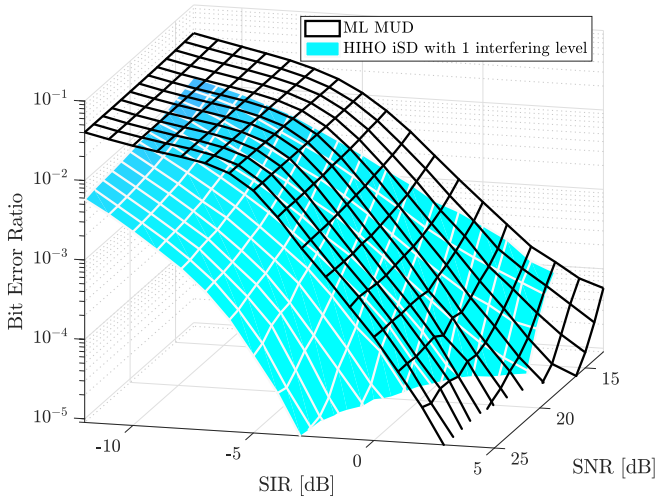

Fig. 11: BER performance with respect to SNR and SIR, when $U = 2$ supported and $U = 15$ interfering aircraft transmit using the same resources. The $U = 2$ users are angularly close to each other and their almost common angular vicinity of $\Phi = 10°$ and there are maximum $U_{\max,AV} = 2$ interferers. The rest of the parameters are gathered in Table II.

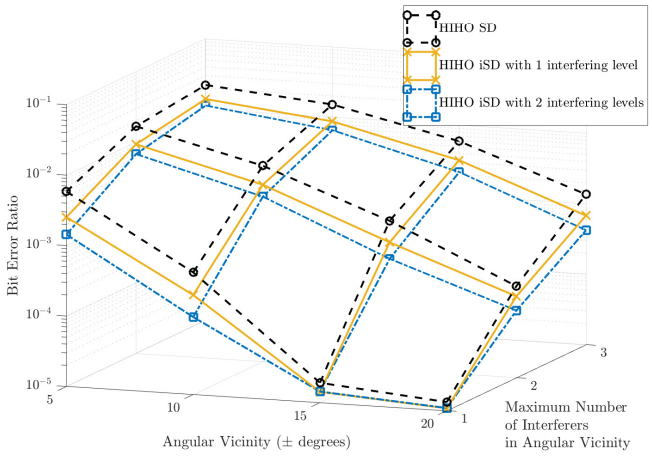

Fig. 12: BER performance with respect to the angular vicinity Φ and the maximum number of interferers in angular vicinity $U_{\max,AV}$, when $U = 2$ supported and $U = 15$ interfering aircraft transmit using the same resources. The two supported aircraft have very different AoAs and we have an SNR value of 17 dB and an SIR value of 0 dB. The rest of the parameters are gathered in Table II.

$U_{\max,AV}$. As expected, allowing up to two interfering levels, $L^{\max}_{intrf} = 2$, further improves the performance of the HIHO iSD. This is true for all the $[\Phi, U_{\max,AV}]$ pairs of Fig. 12, except for the case, where Φ is high and $U_{\max,AV} = 1$, since most of the time, a single common interferer is in the vicinity of both supported aircraft. As expected, this represents the scenario associated with the best performance. For any other $[\Phi, U_{\max,AV}]$ pair in Fig. 12, allowing a higher number of interfering levels in the tree search of the HIHO iSD improves

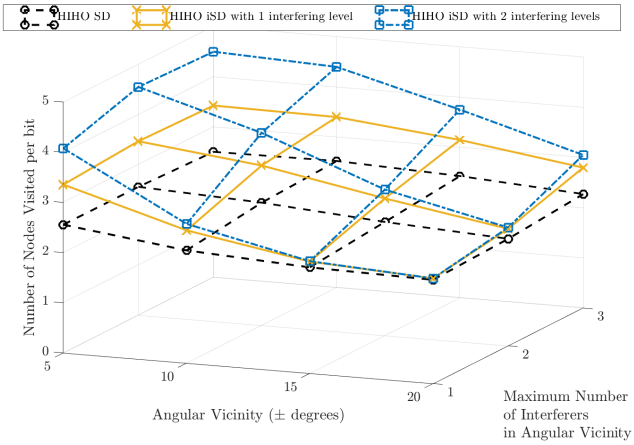

Fig. 13: Number of nosed visited per bit with respect to the angular vicinity Φ and the maximum number of interferers in angular vicinity $U_{\max,AV}$, when $U = 2$ supported and $U = 15$ interfering aircraft transmit using the same resources. The two supported aircraft have very different AoAs and we have an SNR value of 17 dB and an SIR value of 0 dB. The rest of the parameters are gathered in Table II.

the system's BER performance.

However, this comes with an increased complexity requirement, as illustrated in Fig. 13. In more detail, by allowing $L^{\max}_{intrf} = 2$ interfering levels in the HIHO iSD requires a higher computational complexity on average, when compared to the HIHO iSD with a single interfering level, or the conventional HIHO SD. The associated increase in the complexity imposed is higher, when the angular vicinity is low, since in that case the AoAs of more interferers are closer to those of the supported users. In the following discussions, we will be using $L^{\max}_{intrf} = 1$ interfering level at most in the investigated iSDs, since we believe that it strikes a good trade-off between the performance improvement attained and the additional complexity imposed.

When multiple MUD - DES/DEC iterations are allowed at the GS's receiver, we may employ the SISO iSD of Section III-B. In Fig. 14 we have fixed the SNR value to 20 dB and we evaluate the system's BER performance while varying the SIR value for a single and two MUD - DES/DEC iterations, when employing the proposed SISO iSD in conjunction with a single interfering level and the Max-Log-MAP MUD. In order to make the system more challenging for the supported users, we have allowed up to $U_{\max,AV} = 2$ interfering users to rely on the same resources in the angular vicinity of $\Phi = 10°$ of each supported user. We may observe in Fig. 14 that the SISO iSD outperforms the Max-Log-MAP MUD during both the first and second decoding iteration. At a target BER of 10^{-5} the SISO iSD achieves and SIR gain of 2 and 1.5 dB during the first and second decoding iteration, respectively.

The BER performance trends are different, when the SIR is fixed and the SNR is varied. Figure 15 depicts the BER performance of the same system, when the SIR is fixed to -1 dB and the SNR is varied. In the low-SNR region the interfering signals' strength is below the AWGN's power,

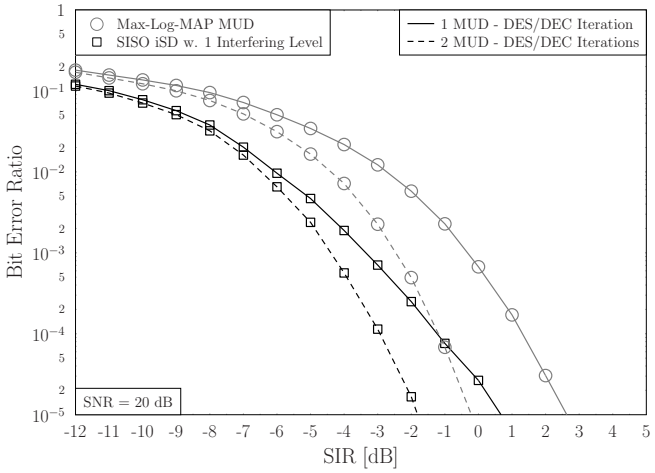

Fig. 14: BER performance with respect to the SIR for a fixed SNR value of 20 dB, when $U = 2$ supported and $U = 15$ interfering aircraft transmit using the same resources. The two supported aircraft have very different AoAs and multiple iterations are allowed at the receiver. There are maximum $U_{\max,AV} = 2$ interferers in each user's angular vicinity of $\Phi = 10°$. The rest of the parameters are gathered in Table II.

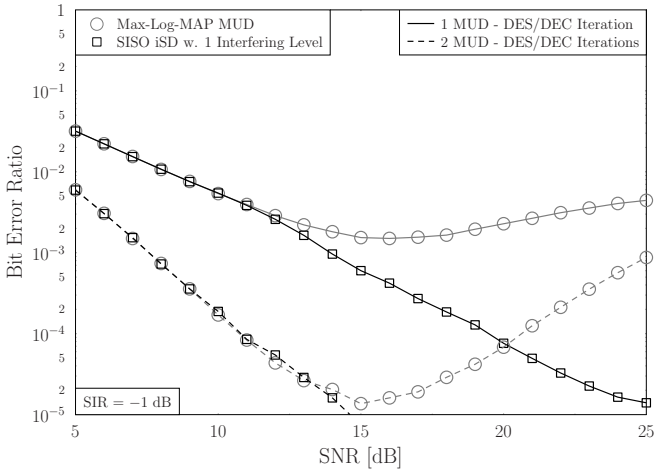

Fig. 15: BER performance with respect to the SNR for a fixed SIR value of -1 dB, when $U = 2$ supported and $U = 15$ interfering aircraft transmit using the same resources. The two supported aircraft have very different AoAs and multiple iterations are allowed at the receiver. There are maximum $U_{\max,AV} = 2$ interferers in each user's angular vicinity of $\Phi = 10°$. The rest of the parameters are gathered in Table II.

therefore the SISO iSD has the same performance as the Max-Log-MAP MUD, since no interfering signals are included in the tree search. As the SNR increases at the same SIR value, the system becomes interference-limited, since the signals of multiple interfering aircraft may end up having a higher power than the thermal noise. Since the SISO iSD takes those signals into consideration, its associated BER continues to decay with the same gradient as that owing to the SNR improvement. By contrast, the system that employs the Max-Log-MAP MUD has a degraded BER performance as the SNR increases, since more and more interfering users' signals have a higher power than the thermal noise's power, when the SNR increases and the SIR remains the same. Since the Max-Log-MAP MUD treats the interference as noise, this leads to the calculation of inaccurate LLR values. Therefore in these regions of operation, the proposed SISO iSD substantially outperforms the Max-Log-MAP MUD.

In Fig. 16 we have plotted the three-dimensional BER performance of the system simulated in Fig. 14 and Fig. 15. As we may observe, similar trends are followed for both the first and for the second MUD - DES/DEC iteration to those in Fig. 14 and Fig. 15 for any fixed SIR or SNR value. More specifically, for any fixed SIR value, the Max-Log-MAP MUD and the SISO iSD have the same performance in the lower-SNR region, but the BER performence of the Max-Log-MAP MUD degrades in the higher-SNR region. Therefore, depending on the operating SNR and assuming a target BER of 10^{-5}, an SIR gain of up to 5 dB is documented in Fig. 16a and an SIR gain of up to 2.5 dB is exhibited, when a second MUD-DES/DEC iteration is allowed.

However, the above gains come at the cost of an increased complexity, as shown in Fig. 17, where the difference between the number of nodes visited by the SISO iSD per bit and their total legitimate number, which is visited by the Max-Log-MAP MUD is plotted. This may be interpreted as additional complexity for the SISO iSD, when the surfaces in Fig. 17 are above the zero-plane indicated, or as reduced complexity, when the surface is below the zero-plane. As we may observe in Fig. 17, the latter only happens in the high-SIR, low-SNR region, where the BER performances of the SISO iSD and of the Max-Log-MAP MUD are equivalent, as verified by Fig. 16. Therefore, in the proposed SISO iSD any performance gain is associated with an increase in the computational complexity. This is in contrast to the proposed HIHO iSD, which may achieve performance gains, while also having a reduced complexity, when compared to the ML MUD. The reason behind this is that in general the conventional depth-first SISO SD visits many more nodes than the depth-first HIHO SD, in order to find the best numerator and denominator of each bit's LLR. Therefore, when we include additional levels in the tree search, its associated complexity may surpass the total number of nodes that the supported levels considered collectively have. As expected, the additional complexity imposed is higher during the second decoding iteration. Moreover, in both decoding iterations, the additional complexity is higher in the low-SIR high-SNR region, since this is the region, where it is more likely that an interfering level will be constantly present in the SISO iSD.

The exchange of information between the MUD and the DES/DEC process may be evaluated using EXIT charts [50]. In Fig. 18 we have plotted the average outer EXIT curve, which corresponds to the DES/DEC operation using an RSC code having a rate of $R = 1/2$ and a spreading factor of $SF = 2$, as well as the average inner EXIT curves of the Max-Log-MAP MUD and the SISO iSD with a single interfering level, for two [SNR, SIR] pairs. The average inner and outer EXIT curves describe the average extrinsic mutual information

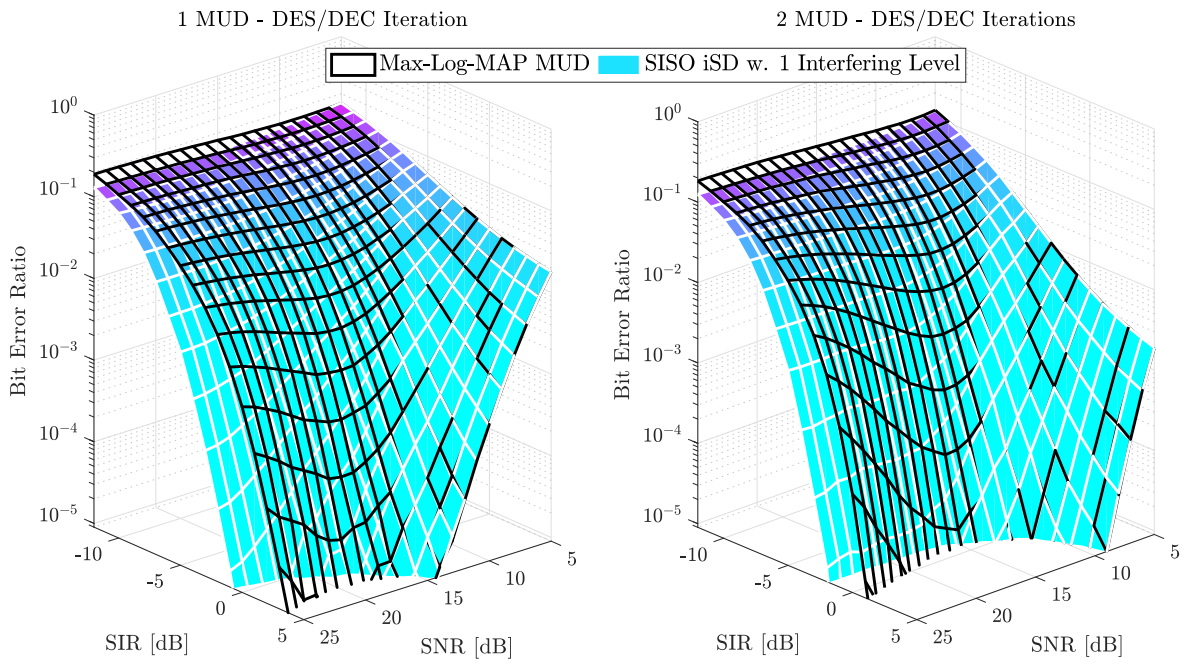

Fig. 16: BER performance with respect to the SNR and the SIR, when $U = 2$ supported and $U = 15$ interfering aircraft transmit using the same resources. The two supported aircraft have very different AoAs and multiple iterations are allowed at the receiver. There are maximum $U_{\max,AV} = 2$ interferers in each user's angular vicinity of $\Phi = 10°$. The rest of the parameters are gathered in Table II.

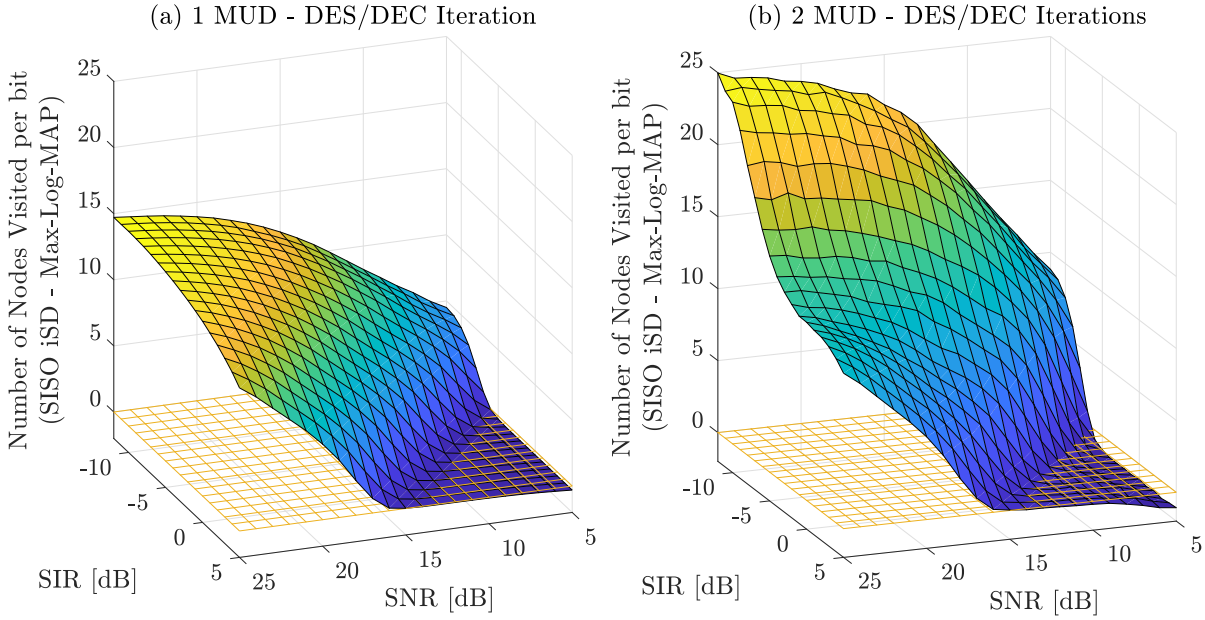

Fig. 17: Number of nodes visited per bit with respect to the SNR and the SIR, when $U = 2$ supported and $U = 15$ interfering aircraft transmit using the same resources. The two supported aircraft have very different AoAs and multiple iterations are allowed at the receiver. There are maximum $U_{\max,AV} = 2$ interferers in each user's angular vicinity of $\Phi = 10°$. The rest of the parameters are gathered in Table II.

at the output of an inner and outer decoder, respectively, when a specific value of *a priori* mutual information is available at their input. The decoding trajectories, which are also plotted in Fig. 18 for the [SNR = 20 dB, SIR = -9 dB] pair, represent the exchange of information between the inner and the outer EXIT curves. When the decoding trajectory reaches the $x = 1$

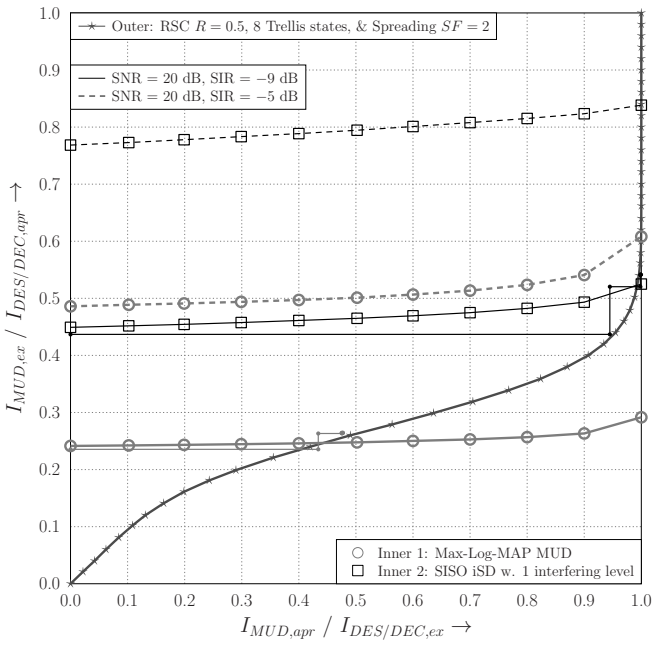

Fig. 18: EXIT chart performance, when $U = 2$ supported and $U = 15$ interfering aircraft transmit using the same resources. The two supported aircraft have very different AoAs and multiple iterations are allowed at the receiver. There are maximum $U_{\max,AV} = 2$ interferers in each user's angular vicinity of $\Phi = 10°$. The rest of the parameters are gathered in Table II.

axis of an EXIT chart in a serially concatenated system like the investigated one, the BER reaches infinitesimally low values. The reason is that the $x = 1$ axis is associated with a unity mutual information at the output of the DES/DEC process, which essentially means that the decoded information bits are the same as the information bits that the supported aircraft wanted to convey to the GS. Therefore, when there is an open tunnel between the inner and the outer decoder's EXIT curves, a near-error-free performance becomes possible, provided that the appropriate number of decoding iterations is employed. From Fig. 18 we may conclude that the proposed SISO iSD outperforms the Max-Log-MAP, since it is either associated with an open tunnel, on average, as is the case when the SIR is equal to -9 dB, or it reaches the $I_{DES/DEC,ex} = 1$ value using fewer decoding iterations, as is the case when the SIR is equal to -5 dB.

V. Conclusions

In this contribution we have investigated diverse A2G scenarios, where the supported and interfering aircraft have been separated either orthogonally or non-orthogonally. The non-orthogonal aircraft transmissions are further separated relying on an adaptive receive beamformer based on whether an aircraft is supported by the GS or not. For the specific cases, where the interfering signals have a higher power than the thermal noise's power, we have proposed a HIHO interference-exploiting SD and a SISO interference-exploiting SD, which are shown to outperform both the conventional HIHO as well as the SISO SDs and hence the ML as well as the Max-Log-MAP MUDs, respectively. At the same time, the SISO iSD requires on average a higher complexity than both the Max-Log-MAP MUD and the SISO SD, while the HIHO iSD requires on average a lower computational complexity than the ML MUD, but at least the same complexity as the HIHO SD. It should be noted that in high-SNR regions the proposed iSDs perform better than their established counterparts, where the interfering signals' power is higher than that of the thermal noise. In the low-SNR regions, the iSDs behave as the conventional depth-first SDs, achieving an optimal performance, while requiring a lower complexity than the ML and Max-Log-MAP MUDs. Based on Figs. 12 and 13, the maximum number of interfering aircraft considered by the iSD should mainly depend on the affordable BER vs complexity trade-off, since allowing more interfering aircraft to have their streams detected would require the tree search to visit more nodes, but it would also result in an improved performance. Hence, again, there is a clear BER vs. complexity trade-off with respect to the angular vicinity and the maximum number of interferers. As a default setting, we would propose to have an angular vicinity equal to the beamformer's angular width to allow the strongest interfering stream to be processed by the iSD, provided that it falls within the angular vicinity parameter chosen.

Our future research is focused on further improving the proposed SISO iSD, by finding a methodology of involving the interfering signals even more beneficially in the decoding iterations, in order to make them contribute even more fruitfully in iterative receivers by updating their *a priori* LLRs. Furthermore, we are planning to use the proposed A2G system as the backhaul block of routing applications in AANETs.

References

[1] J. Zhang, T. Chen, S. Zhong, W. Zhang, X. Zuo, J. Darlington, A. Payne, R. Maunder, and L. Hanzo, "A Survey of Aeronautical Ad-Hoc Networking," *IEEE Communications Surveys & Tutorials, (submitted)*, 2018.

[2] A. Jahn, M. Holzbock, J. Muller, R. Kebel, M. de Sanctis, A. Rogoyski, E. Trachtman, O. Franzrahe, M. Werner, and F. Hu, "Evolution of Aeronautical Communications for Personal and Multimedia Services," *IEEE Communications Magazine*, vol. 41, pp. 36–43, July 2003.

[3] D. Medina, F. Hoffmann, F. Rossetto, and C. H. Rokitansky, "A Geographic Routing Strategy for North Atlantic In-Flight Internet Access Via Airborne Mesh Networking," *IEEE/ACM Transactions on Networking*, vol. 20, pp. 1231–1244, Aug 2012.

[4] Q. Vey, A. Pirovano, J. Radzik, and F. Garcia, *Aeronautical Ad Hoc Network for Civil Aviation*, pp. 81–93. Cham: Springer International Publishing, 2014.

[5] D. Medina, F. Hoffmann, F. Rossetto, and C. H. Rokitansky, "Routing in the Airborne Internet," in *2010 Integrated Communications, Navigation, and Surveillance Conference Proceedings*, pp. A7–1–A7–10, May 2010.

[6] M. Schnell and S. Scalise, "NEWSKY - Concept for NEtWorking the SKY for Civil Aeronautical Communications," *IEEE Aerospace and Electronic Systems Magazine*, vol. 22, pp. 25–29, May 2007.

[7] D. Medina, *Geographic Load Share Routing in the Airborne Internet*. PhD thesis, Paris Lodron Universität Salzburg, July 2011.

[8] M. Royer, A. Pirovano, and F. Garcia, "Survey on Context-Aware Publish/Subscribe Systems for VANET," in *Communication Technologies for Vehicles*, pp. 46–58, Springer Berlin Heidelberg, 2013.

[9] EUROCONTROL, "Aircraft Communications, Addressing and Reporting System," http://www.skybrary.aero/index.php/Aircraft Communications, Addressing and Reporting System, (Available Online).

[10] I. Aviation Spectrum Resources, "Selective Calling (SELCAL) Users Guide," https://www.asri.aero/wp- content/uploads/2012/07/ 110914-ASRI-SELCAL-Users-Guide-61742-Rev-C.pdf, 2013, (Available Online).

[11] EUROCONTROL, "L-DACS1 System Definition Proposal: Deliverable D3 Specifications for L-DACS1 Prototype," http://www.eurocontrol.int/sites/default/files/article/content/documents/communications/ 01042009-ldacs1- d3- v10.pdf, 2009, (Available Online).

[12] EUROCONTROL, "L-DACS1 System Definition Proposal: Deliverable D2," http://www.eurocontrol.int/sites/default/files/article/content/documents/communications/d2- final- l- dacs1- spec- proposal- v10.pdf, 2009, (Available Online).

[13] C. H. Rokitansky, M. Ehammer, M. Schnell, S. Brandes, S. Gligorevic, C. Rihacek, and M. Sajatovic, "B-AMC A System for Future Broadband Aeronautical Multi-Carrier Communications in the L-BAND," in *IEEE/AIAA 26th Digital Avionics Systems Conference*, pp. 4.D.2–1–4.D.2–13, 2007.

[14] K. Etemad, "Overview of Mobile WiMAX Technology and Evolution," *IEEE Communications Magazine*, vol. 46, no. 10, pp. 31–40, 2008.

[15] EUROCONTROL, "L-DACS2 System Definition Proposal: Deliverable D2," https://www.eurocontrol.int/sites/default/files/article/content/documents/communications/11052009-ldcas2-d2-deliverable-v1.0.pdf, 2009, (Available Online).

[16] EUROCONTROL, "L-DACS2 Transmitter and Receiver Prototype Equipment Specifications: Deliverable D3," http://www.eurocontrol.int/sites/default/files/article/content/documents/communications/18062009-ldacs2- design- d3- v1.2.pdf, 2009, (Available Online).

[17] Inmarsat, "The European Aviation Network (EAN)," https://www.inmarsat.com/aviation/aviation- connectivity- services/european- aviation- network/, 2017, (Available Online).

[18] Inmarsat, "ATG4 Coverage," https://www.gogoair.com/commercial/atg4, (Available Online).

[19] Y. Saito, Y. Kishiyama, A. Benjebbour, T. Nakamura, A. Li, and K. Higuchi, "Non-Orthogonal Multiple Access (NOMA) for Cellular Future Radio Access," in *IEEE Vehicular Technology Conference (VTC Spring)*, pp. 1–5, June 2013.

[20] Z. Ding, Z. Yang, P. Fan, and H. V. Poor, "On the Performance of Non-Orthogonal Multiple Access in 5G Systems with Randomly Deployed Users," *IEEE Signal Processing Letters*, vol. 21, pp. 1501–1505, Dec 2014.

[21] L. Dai, B. Wang, Y. Yuan, S. Han, C. l. I, and Z. Wang, "Non-Orthogonal Multiple Access for 5G: Solutions, Challenges, Opportunities, and Future Research Trends," *IEEE Communications Magazine*, vol. 53, pp. 74–81, September 2015.

[22] Z. Yang, Z. Ding, P. Fan, and G. K. Karagiannidis, "On the Performance of Non-orthogonal Multiple Access Systems With Partial Channel Information," *IEEE Transactions on Communications*, vol. 64, pp. 654–667, Feb 2016.

[23] Z. Ding, Y. Liu, J. Choi, Q. Sun, M. Elkashlan, C. L. I, and H. V. Poor, "Application of Non-Orthogonal Multiple Access in LTE and 5G Networks," *IEEE Communications Magazine*, vol. 55, pp. 185–191, February 2017.

[24] L. Hanzo, Y. Akhtman, M. Jiang, and L. Wang, *MIMO-OFDM for LTE, WIFI and WIMAX: Coherent versus Non-Coherent and Cooperative Turbo-Transceivers*. John Wiley & Sons, 2010.

[25] M.-O. Damen, H. El-Gamal, and G. Caire, "On maximum-likelihood detection and the search for the closest lattice point," *Information Theory, IEEE Transactions on*, vol. 49, no. 10, pp. 2389–2402, 2003.

[26] E. Agrell, T. Eriksson, A. Vardy, and K. Zeger, "Closest Point Search in Lattices," *IEEE Transactions on Information Theory*, vol. 48, no. 8, pp. 2201–2214, 2002.

[27] E. Viterbo and J. Boutros, "A Universal Lattice Code Decoder for Fading Channels," *IEEE Transactions on Information Theory*, vol. 45, pp. 1639–1642, Jul 1999.

[28] B. Hassibi and B. Hochwald, "Linear Dispersion Codes," in *IEEE International Symposium on Information Theory*, p. 325, 2001.

[29] A. Wolfgang, J. Akhtman, S. Chen, and L. Hanzo, "Iterative MIMO Detection for Rank-Deficient Systems," *IEEE Signal Processing Letters*, vol. 13, no. 11, pp. 699–702, 2006.

[30] C. Studer and H. Bolcskei, "Soft-Input Soft-Output Single Tree-Search Sphere Decoding," *IEEE Transactions on Information Theory*, vol. 56, pp. 4827–4842, Oct 2010.

[31] L. Hanzo, O. Alamri, M. El-Hajjar and N. Wu, *Near-Capacity Multi-Functional MIMO Systems: Sphere-Packing, Iterative Detection and Cooperation*. John Wiley & Sons, IEEE Press, May 2009.

[32] J. Litva and T. K. Lo, *Digital Beamforming in Wireless Communications*. Norwood, MA, USA: Artech House, Inc., 1st ed., 1996.

[33] S. Chen, A. Wolfgang, C. J. Harris, and L. Hanzo, "Symmetric RBF Classifier for Nonlinear Detection in Multiple-Antenna-Aided Systems," *IEEE Transactions on Neural Networks*, vol. 19, pp. 737–745, May 2008.

[34] A. Wolfgang, S. Chen, and L. Hanzo, "Radial Basis Function Aided Space-Time Equalization in Dispersive Fading Uplink Environments," in *2005 IEEE 61st Vehicular Technology Conference*, vol. 3, pp. 1552–1556, May 2005.

[35] M. A. Richards, ed., *Principles of Modern Radar: Basic principles*. Radar, Sonar & Navigation, Institution of Engineering and Technology, 2010.

[36] S. Blackman and R. Popoli, *Design and Analysis of Modern Tracking Systems*. Artech House radar library, Artech House, 1999.

[37] Y. Bar-Shalom and L. A. U. E. University of California, *Multitarget-multisensor Tracking: Applications and Advances*. No. v. 1 in Artech House radar library, Artech House, 1990.

[38] L. Ping, "Interleave-Division Multiple Access and Chip-by-Chip Iterative Multi-User Detection," *IEEE Communications Magazine*, vol. 43, pp. S19–S23, June 2005.

[39] L. Ping, L. Liu, K. Wu, and W. K. Leung, "Interleave Division Multiple-Access," *IEEE Transactions on Wireless Communications*, vol. 5, pp. 938–947, April 2006.

[40] R. Zhang and L. Hanzo, "Three Design Aspects of Multicarrier Interleave Division Multiple Access," *IEEE Transactions on Vehicular Technology*, vol. 57, pp. 3607–3617, November 2008.

[41] R. Zhang, L. Xu, S. Chen, and L. Hanzo, "EXIT-Chart-Aided Hybrid Multiuser Detector for Multicarrier Interleave-Division Multiple Access," *IEEE Transactions on Vehicular Technology*, vol. 59, pp. 1563–1567, March 2010.

[42] J. Dang, W. Zhang, L. Yang, and Z. Zhang, "OFDM-IDMA with User Grouping," *IEEE Transactions on Communications*, vol. 61, pp. 1947–1955, May 2013.

[43] P. Botsinis, D. Alanis, Z. Babar, S. Ng, and L. Hanzo, "Iterative Quantum-Assisted Multi-User Detection for Multi-Carrier Interleave Division Multiple Access Systems," *IEEE Transactions on Communications*, vol. 63, pp. 3713–3727, July 2015.

[44] P. Botsinis, I. Hemadeh, D. Alanis, Z. Babar, H. Nguyen, D. Chandra, S. X. Ng, M. El-Hajjar, and L. Hanzo, "Joint-Alphabet Space Time Shift Keying in mm-Wave Non-Orthogonal Multiple Access," *IEEE Access*, vol. PP, no. 99, pp. 1–1, 2017.

[45] Y. Liu, Z. Qin, M. Elkashlan, Z. Ding, A. Nallanathan, and L. Hanzo, "Nonorthogonal Multiple Access for 5G and Beyond," *Proceedings of the IEEE*, vol. 105, pp. 2347–2381, Dec 2017.

[46] E. Haas, "Aeronautical Channel Modeling," *IEEE Transactions on Vehicular Technology*, vol. 51, pp. 254–264, Mar 2002.

[47] A. Neul, J. Hagenauer, W. Papke, F. Dolainsky, and F. Edbauer, "Propagation Measurements for the Aeronautical Satellite Channel," in *IEEE Vehicular Technology Conference*, vol. 37, pp. 90–97, June 1987.

[48] S. M. Elnoubi, "A Simplified Stochastic Model for the Aeronautical Mobile Radio Channel," in *Vehicular Technology Society Conference - Frontiers of Technology*, pp. 960–963, May 1992.

[49] Z. Wang, W. Liu, C. Qian, S. Chen, and L. Hanzo, "Two-Dimensional Precoding for 3-D Massive MIMO," *IEEE Transactions on Vehicular Technology*, vol. 66, pp. 5485–5490, June 2017.

[50] M. El-Hajjar and L. Hanzo, "EXIT Charts for System Design and Analysis," *IEEE Communications Surveys & Tutorials*, vol. 16, pp. 127–153, January 2014.